

*Digital Comprehensive Summaries of Uppsala Dissertations  
from the Faculty of Pharmacy 355*

# Magnetic nanoparticles for diagnosis of inflammatory bowel disease

SHNO ASAD



ACTA UNIVERSITATIS  
UPSALIENSIS  
2024

ISSN 1651-6192  
ISBN 978-91-513-2164-6  
urn:nbn:se:uu:diva-532431



UPPSALA  
UNIVERSITET

Dissertation presented at Uppsala University to be publicly examined in room A1:111a, BMC, Husargatan 3, Uppsala, Friday, 6 September 2024 at 13:15 for the degree of Doctor of Philosophy (Faculty of Pharmacy). The examination will be conducted in English. Faculty examiner: Associate Professor Bruno Sarmiento (i3S - Instituto de Investigação e Inovação em Saúde, Universidade do Porto).

### **Abstract**

Asad, S. 2024. Magnetic nanoparticles for diagnosis of inflammatory bowel disease. *Digital Comprehensive Summaries of Uppsala Dissertations from the Faculty of Pharmacy* 355. 68 pp. Uppsala: Acta Universitatis Upsaliensis. ISBN 978-91-513-2164-6.

The identification of biomarkers overexpressed during inflammation is critical for targeting diagnostic or therapeutic agents to the inflamed intestine in inflammatory bowel disease (IBD). The first part of this thesis employs global proteomic analysis to identify preclinical IBD biomarkers using in vitro and in vivo models. The study focuses on apical plasma membrane biomarkers and secreted biomarkers, identifying promising targets for diagnostic imaging probes. Proteomic analysis quantified 7340 proteins across ileum, proximal, and distal colon samples in vivo, revealing significant protein concentration changes primarily in the colon after DSS treatment. Functional annotation linked these changes to inflammatory responses. In vitro analysis using Caco-2 cells treated with TNF- $\alpha$  identified 465 proteins involved in defense and cytokine responses, showing greater relevance for modeling inflammation than DSS-treated cells.

Key inflammatory biomarkers were identified, including TGM2, ICAM1, CEACAM1, and ANXA1, with varied upregulation across models. These biomarkers were validated via immunohistochemistry, showing consistent expression in inflamed and healthy tissues. Additionally, luminal and immune cell-associated proteins such as myeloperoxidase and calprotectin were identified, suggesting their potential for in situ quantitative assessment of IBD activity.

The second part of this thesis details the development of MRI-active biosensors using superparamagnetic iron oxide nanoparticles (SPIONs) functionalized via click chemistry with ligands targeting the identified biomarkers. The synthesis and characterization of SiO<sub>2</sub>-coated  $\gamma$ -Fe<sub>2</sub>O<sub>3</sub> SPIONs and their subsequent functionalization with antibodies targeting ICAM1 were optimized for enhanced biocompatibility and targeting efficacy. In vitro studies demonstrated specific binding and internalization of bioconjugated SPIONs in inflamed Caco-2 cells.

The third part explores in vivo targeting efficacy of bioconjugated SPIONs in colitis-induced mice. Ceacam1-conjugated SPIONs showed significant binding to inflamed tissues, highlighting their potential for targeted imaging and therapeutic delivery in IBD. This thesis underscores the importance of systematic nanoparticle modification and characterization, advancing precision medicine and diagnostic technologies for IBD.

*Keywords:* inflammatory bowel disease, proteomics, biomarkers, SPIONs, click chemistry, MRI biosensors, targeted therapy, diagnostic imaging

*Shno Asad, Department of Pharmacy, Box 580, Uppsala University, SE-75123 Uppsala, Sweden.*

© Shno Asad 2024

ISSN 1651-6192

ISBN 978-91-513-2164-6

URN urn:nbn:se:uu:diva-532431 (<http://urn.kb.se/resolve?urn=urn:nbn:se:uu:diva-532431>)

بۆ داڭكۆم و باوكۆم

*Bo daykm û bawkm*

“The heart became an ocean of knowledge,  
yet I do not understand the alphabet”  
Mahwi

# List of Papers

This thesis is based on the following papers, which are referred to in the text by their Roman numerals.

- I. **Asad, S.\***, Wegler, C.\*, Ahl, D., Bergström, C.A.S., Phillipson, M., Artursson, P., Teleki, A. (2021) Proteomics-informed identification of luminal targets for *in situ* diagnosis of inflammatory bowel disease. *Journal of Pharmaceutical Science*, 110 (1): 239-250
- II. **Asad, S.**, Ahl, D., Suárez-López, Y.C., Erdélyi, M., Phillipson, M., Teleki, A. (2024) Click chemistry-based bioconjugation of magnetic nanoparticles. *Under revision*
- III. **Asad, S.\***, Ahl, D.\*, M Phillipson, Teleki, A. Bioconjugated nanoparticles as targeted MRI contrast agents for diagnosis of ulcerative colitis. *Manuscript*

Reprints were made with permission from the respective publishers.

*\*The authors contributed equally to this work.*

## Other contributions

- I. **Asad, S.\***, Jacobsen, A.C.\*, Teleki, A. (2021) Inorganic Nanoparticles for Oral Drug Delivery: Opportunities, Barriers and Future Perspectives. *Current Opinion in Chemical Engineering*, 38: 100869
- II. Ansari, S.R., Hempel, N.J., **Asad, S.**, Svedlindh, P., Bergström, C.A.S., Löbmann, K., Teleki, A. (2022) Hyperthermia-induced in situ drug amorphization by superparamagnetic nanoparticles in oral dosage forms. *ACS Applied Materials & Interfaces*, 14 (19): 21978-21988
- III. Hempel, N.J., Merkl, P., **Asad, S.**, Knopp, M.M., Berthelsen, R., Bergström, C.A.S., Teleki, A., Sotiriou G.A., Löbmann, K. (2021) Utilizing laser-activation of photothermal plasmonic nanoparticles to induce on-demand drug amorphization inside a tablet, *Molecular Pharmaceutics*, 88 (6): 2254-2262

# Contents

Introduction.....	11
Inflammatory bowel disease.....	11
Magnetic nanoparticles .....	14
Superparamagnetic iron oxide nanoparticles for MRI.....	15
Synthesis of magnetic nanoparticles .....	16
Bioconjugation of nanoparticles.....	17
Aim of the thesis .....	20
Methods .....	21
Synthesis of iron oxide nanoparticles.....	21
Flame spray pyrolysis.....	21
Functionalization of nanoparticles .....	22
Silanization .....	22
Synthesis of alkyne-containing linker.....	22
Introducing a click-handle .....	22
Antibody conjugation .....	23
Physicochemical characterization of nanoparticles.....	24
X-ray diffraction .....	25
Attenuated total reflectance Fourier-transform Infrared spectroscopy .....	25
Transmission Light Microscopy .....	25
Thermogravimetric analysis .....	25
Dynamic light scattering.....	25
Sodium dodecyl-sulphate polyacrylamide gel electrophoresis.....	26
Quantification of functional groups.....	26
<i>In vitro</i> methods .....	27
<i>In vitro</i> IBD model.....	27
Cell viability after exposure to functionalized SPIONs.....	27
Binding efficacy of bioconjugated SPIONs <i>in vitro</i> .....	28
Staining of filter-grown Caco-2 cells.....	28
<i>In vivo</i> methods .....	29
<i>In vivo</i> IBD model .....	29
Administration of bioconjugated SPIONs <i>in vivo</i> .....	30
Tissue biopsy sampling for proteomics .....	30
Global proteomics analysis .....	31

Data Analysis and Bioinformatics.....	31
Analysis of <i>in vitro</i> and <i>in vivo</i> samples.....	33
Immunohistochemical analysis.....	33
Inductively coupled plasma optical emission spectroscopy .....	33
Confocal microscopy .....	33
Magnetic resonance imaging .....	34
Results and discussion .....	35
Proteomics-based identification of targets for <i>in situ</i> targeting of IBD (Paper I).....	35
Global proteomics analysis of <i>in vivo</i> IBD model.....	35
Global proteomics analysis of <i>in vitro</i> IBD model .....	36
Identification of inflammatory biomarkers.....	37
Click chemistry-based bioconjugation of SPIONs (Paper II) .....	42
SPION synthesis and coating.....	42
Surface functionalization of SPIONs.....	42
Targeting capability of bioconjugated SPIONs <i>in vitro</i> .....	45
Targeting efficacy of bioconjugated nanoparticles colitis-induced mice (Paper III) .....	48
Introduction of carboxylic acid moieties .....	48
Antibody affinity and <i>in vivo</i> targeting.....	50
Targeting efficacy <i>in vivo</i> .....	51
Conclusions.....	57
Future perspectives .....	59
Acknowledgements.....	61
References.....	65

# Abbreviations

APTES	(3-Aminopropyl)triethoxysilane
ATR-FTIR	Attenuated total reflectance Fourier transform infrared
CFP	Cyan fluorescent protein
CT	Computed tomography
CuAAC	Copper-catalyzed azide-alkyne cycloaddition
DAI	Disease activity index
DBCO	Dibenzocyclooctyne
DLS	Dynamic light scattering
DMEM	Dulbecco's modified eagle serum
DSS	Dextran sulphate sodium
EDC	1-ethyl-3-(3-dimethylaminopropyl)carbodiimide
FBS	Fetal bovine serum
FSP	Flame spray pyrolysis
GI	Gastrointestinal
IBD	Inflammatory bowel disease
ICP-OES	Inductively coupled plasma - optical emission spectroscopy
MRI	Magnetic resonance imaging
NEAA	Non-essential amino acids
NHS	N-hydroxysuccinimide
PBS	Phosphate-buffered saline
PCA	Principal component analysis
SDS-PAGE	Sodium dodecyl-sulphate polyacrylamide gel electrophoresis
SPAAC	Strain-promoted azide-alkyne cycloaddition
SPIONs	Superparamagnetic iron oxide nanoparticles
TEM	Transmission electron microscopy
TGA	Thermogravimetric analysis
TNF- $\alpha$	Tumour Necrosis Factor- $\alpha$
XRD	X-ray diffraction



# Introduction

Nanomedicine has profoundly transformed the landscape of medical diagnostics, treatment, and drug delivery. By utilizing nanoparticles, which typically range from 0.1 to 100 nanometers in size, therapeutic efficacy and precision can be enhanced.<sup>[1,2]</sup> A defining feature of nanomaterials is their large surface-to-volume ratio, which significantly increases their chemical reactivity compared to their corresponding bulk materials. This heightened reactivity is due to a greater proportion of atoms being exposed on the surface, allowing for enhanced interaction with biological targets.<sup>[3]</sup> These particles can be engineered to deliver drugs directly to targeted cells, minimizing side effects and improving patient outcomes. Additionally, their use in diagnostic imaging and disease monitoring offers unprecedented accuracy and early detection capabilities. As research advances, nanomedicine holds the promise of revolutionizing personalized medicine, enabling tailored treatments that address the specific needs of individual patients.

Today, clinically approved nanoparticle-based formulations such as Doxil®, Abraxane®, and Feraheme®, are being used to treat a range of conditions from cancer to iron deficiency, highlighting the practical utility of nanoparticle-based therapeutics.<sup>[4]</sup> Additionally, the success of nanoparticle-based mRNA vaccines for COVID-19 has further underscored the vast potential of nanomedical innovations. Hence, the utility of nanomedical products as drug delivery vehicles has become widely adopted and well-understood over the past years, but there is a yet clinically unacknowledged potential of using nanoparticles, particularly metal-based particles, for diagnosing and monitoring diseases that can be locally targeted in the gastrointestinal (GI) tract, such as colon cancer or inflammatory bowel disease (IBD).

## Inflammatory bowel disease

Inflammatory bowel disease (IBD) encompasses a group of chronic inflammatory conditions of the GI tract, including Crohn's disease and ulcerative colitis. Common symptoms of IBD include abdominal pain, diarrhoea, rectal bleeding, weight loss and perianal disease that typically presents with alternating periods of flare-ups and remissions.<sup>[5]</sup> The exact cause of IBD remains unclear, however it is suggested to result from an uncontrolled immune

response to a trigger in genetically predisposed individuals.<sup>[6,7]</sup> Changes in the gut microbiome and environmental factors are often suggested as potential causes of this immune response, however, it continues to be a topic of debate.<sup>[6]</sup>

The incidence of IBD has steadily increased in the Western countries during the twentieth century, leading to its perception as a Western disease. However, recent data shows an alarming increase of IBD cases in developing and newly industrialized countries, indicating its emergence as a global issue (Figure 1).<sup>[7-9]</sup> The economic impact of IBD is significant, and managing the disease is challenging due to its incurability, requiring continuous medication. As a result, the rising global prevalence of IBD is expected to place a significant socioeconomic burden on governments and health care systems in the coming years.<sup>[6]</sup>

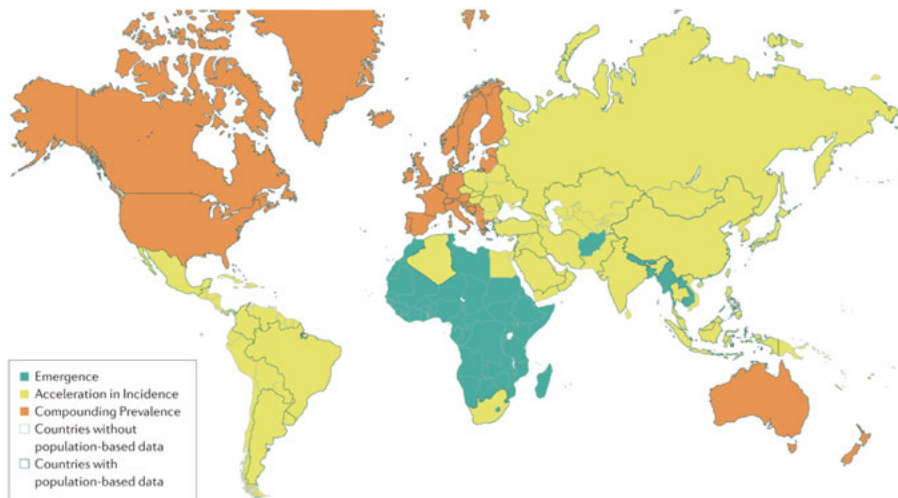


*Figure 1. Global map depicting different epidemiological stages of IBD progression in 2020, highlighting the areas where IBD is emerging (green), accelerating in incidence (yellow) and compounding prevalence (orange). Reprinted with permission from Nature Reviews Gastroenterology & Hepatology © 2020, Springer Nature.<sup>[9]</sup>*

Both the treatment and diagnosis of IBD face significant challenges. Traditional treatments focus on symptom management using aminosalicylates, corticosteroids, immunomodulators, and biologics, along with general supportive measures and surgical resection when needed.<sup>[10]</sup> However, a significant number of patients either do not respond to these treatments or lose responsiveness over time, highlighting the need for new therapeutic strategies.<sup>[10]</sup> Immense research efforts have been invested to enhance current IBD therapies and to develop new approaches. These efforts have led to the development of several promising products in the pipeline, including orally administered Janus kinase

inhibitors, anti-adhesion agents, anti-trafficking agents and stem cell therapy.<sup>[10-12]</sup>

In contrast, the diagnosis of IBD has seen little improvement. Currently, IBD diagnosis relies on a combination of biological and morphological tests (Figure 2), including GI endoscopies with mucosal biopsies. Depending on whether Crohn's disease or ulcerative colitis is suspected, either an upper endoscopy or colonoscopy is typically performed. This invasive procedure is unpopular among patients and carry substantial healthcare costs.

Although GI endoscopy is the current gold standard, it often falls short in providing an accurate diagnosis. As a result, patients frequently endure symptoms for several months before receiving a definitive IBD diagnosis.<sup>[13,14]</sup> Such delays cause significant pain and discomfort, preventing timely and appropriate medical treatment.

Furthermore, blood parameters, such as C-reactive protein, erythrocyte sedimentation rate, serum albumin, platelet count, and hemoglobin levels, are commonly used as supplementary biomarkers to assess IBD.<sup>[15]</sup> Similarly, faecal biomarkers, such as calprotectin, lactoferrin, and myeloperoxidase, have been identified for analysing faeces samples to determine disease activity.<sup>[16]</sup> Although analysing faecal samples is less invasive compared to GI endoscopy, both approaches are currently used only as complementary tools to endoscopic measures, as they do not provide spatiotemporal information about the disease. Additionally, commonly used biomarkers like calprotectin are not specific to IBD and can be associated with other GI diseases such as neoplasia, infections, and celiac disease.<sup>[16]</sup>

To evaluate parts of the intestine that are inaccessible to endoscopic evaluation, advanced imaging techniques such as computed tomography (CT) and magnetic resonance imaging (MRI) have traditionally been employed. CT scanning has the notable disadvantage to involve exposure to ionizing radiation, which is particularly concerning for patients with IBD, who require frequent assessments due to the relapsing nature of their condition. On the contrary, MRI presents a compelling alternative for GI imaging, offering detailed tissue visualization without the associated risks of radiation exposure. Patients are administered contrast agents prior to the scan, which enhance the visibility of internal structures, tissues, and abnormalities, providing clearer MRI images. For the assessment of IBD, adequate bowel distension is crucial, as collapsed bowel loops can obscure lesions or create false impressions of a thickened bowel wall.<sup>[17,18]</sup> Bowel distension is typically achieved by administering contrast solutions either orally or through mid-gut tubing, with the latter providing more consistent results but being unpleasant and time-consuming.<sup>[17]</sup> A variety of contrast agents are available, each with its own advantages and drawbacks, all designed to enhance the visualization in the GI tract. However, these agents do not directly provide a clear delineation of the disease activity. In addition, current contrast agents, while useful for detecting tissue abnormalities, lack specificity and can identify changes caused by conditions

other than IBD. This limitation, along with the current delay of final diagnosis underscores the need for developing reliable, patient-friendly diagnostic tools that can improve the accuracy and specificity of IBD detection.

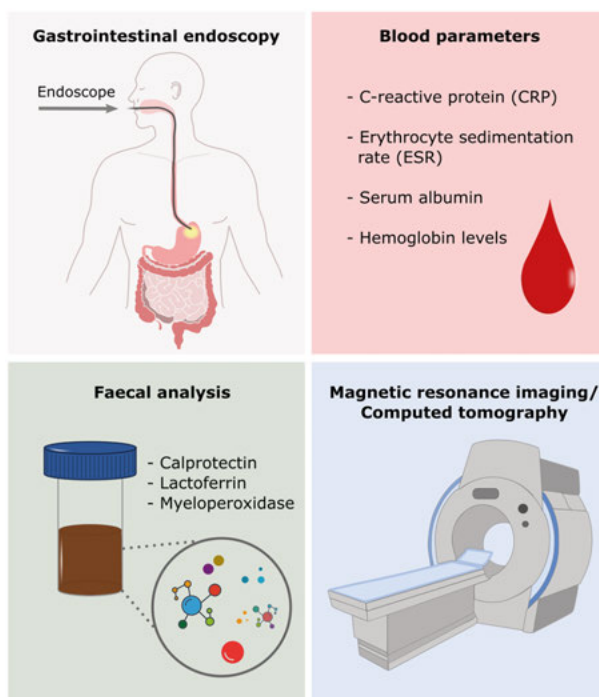


*Figure 2.* Current procedures for diagnosing IBD involve a combination of different strategies to estimate disease activity. These include GI endoscopies, blood-related tests, faecal analysis and imaging techniques such as MRI and CT.

## Magnetic nanoparticles

Magnetic nanoparticles are often composed of magnetic materials such as iron oxide ( $\text{Fe}_3\text{O}_4$  or  $\gamma\text{-Fe}_2\text{O}_3$ ), cobalt, or nickel. These particles have immense potential in several advanced medical applications, including hyperthermia cancer therapy and as contrast agents for MRI.<sup>[19,20]</sup>

Depending on the size, magnetic nanoparticles can exhibit a unique property called superparamagnetism. This phenomenon is observed in small ferromagnetic or ferrimagnetic nanoparticles, where the entire particle acts as a single magnetic domain.<sup>[21]</sup> When exposed to an external magnetic field, superparamagnetic nanoparticles become magnetized, aligning their magnetic moments with the field. However, unlike larger ferromagnetic particles, they do not retain magnetization once the external field is removed. This lack of residual magnetism prevents the particles from magnetic agglomeration,

which is a significant advantage in various biomedical applications. Furthermore, the ability to customize the surface architecture of nanoparticles with various ligands, such as antibodies, peptides, and small molecules, makes them highly versatile tools for controlled and targeted pharmacological applications.

## Superparamagnetic iron oxide nanoparticles for MRI

Through their unique properties, superparamagnetic iron oxide nanoparticles (SPIONs) have contributed to enhancing medical imaging, enabling targeted drug delivery, advancing cancer treatment, improving biosensing, diagnostics and tissue engineering.<sup>[22,23]</sup> For instance, in tissue engineering, SPIONs can be used to create scaffolds that promote cell growth and tissue regeneration.<sup>[24,25]</sup> In hyperthermia cancer therapy, these nanoparticles can be engineered to absorb specific wavelengths of light or electromagnetic radiation, generating heat that selectively destroys cancer cells.<sup>[21,26]</sup> Similarly, in MRI, SPIONs can serve as contrast agents, enhancing the imaging of specific tissues or pathological areas.<sup>[27]</sup>

In MRI, a strong magnetic field aligns the magnetic moments of water protons in the body with the direction of the applied magnetic field (Figure 3a).<sup>[28]</sup> The protons are then excited by a radiofrequency pulse, causing the magnetic moments to spin out of equilibrium (Figure 3b). Once the pulse is removed, the spins will realign with the magnetic field, resulting in an energy release. This released energy and the time it takes to realign with the magnetic field is detected and translated into a computer-assisted image.<sup>[29]</sup> Proton relaxation time is classified by two different processes (Figure 3c, d); longitudinal relaxation (T1), which produces bright, positive contrast, and transverse relaxation (T2), which produces dark, negative contrast.<sup>[30]</sup> Contrast agents, such as SPIONs, are used to shorten the relaxation time and thereby enhance the contrast in MRI images. The superparamagnetic behaviour of SPION gives them high relaxivity values, particularly affecting T2 relaxation.

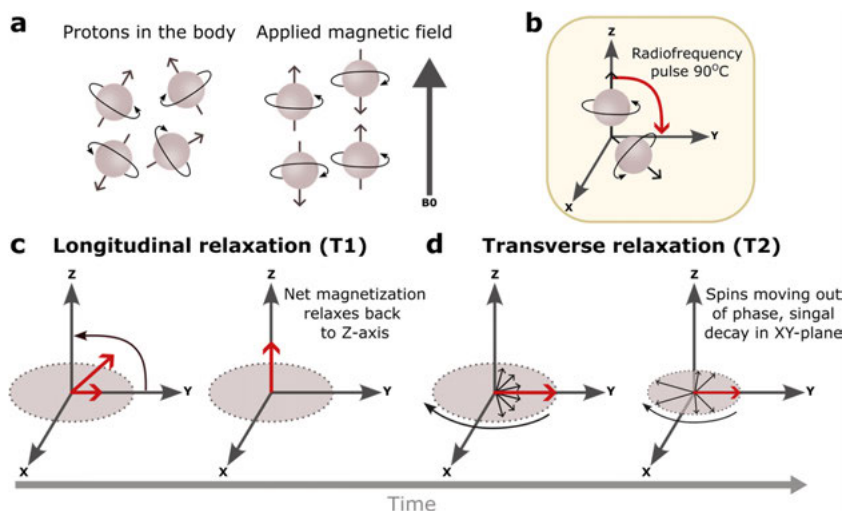


*Figure 3.* T1 and T2 relaxation in MRI. (a) Protons from water molecules in the body align parallel or anti-parallel to the applied external magnetic field. (b) A radiofrequency pulse is applied to flip the net magnetization into the XY-plane. (c) T1 relaxation refers to the time it takes for protons in tissues to realign with the external magnetic field after being disturbed by a radiofrequency pulse. It represents the recovery of longitudinal magnetization. (d) T2 relaxation refers to the time it takes for protons to lose phase coherence among themselves due to interactions with neighbouring protons, representing the decay of transverse magnetization.

Despite the development of SPION-based contrast agents for MRI, their clinical utility has been inconsistent. Several SPION-based agents, such as Feridex® and Resovist® for liver imaging, and Lumirem® for GI imaging, have been approved and marketed. However, their availability is limited to a few countries due to low market uptake.<sup>[31]</sup> Thus, while SPIONs have demonstrated good tolerability and safety, they have not yet achieved widespread clinical use, indicating that their full potential in medical imaging remains untapped.

## Synthesis of magnetic nanoparticles

Despite the successful commercialization of several nanomedical products, the clinical application of metal-based nanomaterials remains limited due to challenges in achieving reproducibility in large-scale production. Methods for synthesizing superparamagnetic iron oxide nanoparticles (SPIONs) can be categorized into physical, wet chemical, and gas phase methods, each offering distinct advantages and drawbacks.<sup>[32]</sup>

The physical method for producing SPIONs is a top-down approach that breaks down large particles into nanoparticles. Techniques such as powder milling, ball milling, and electron beam lithography are commonly used.

Although this method is suitable for large-scale production, it does not allow easy control over the particle sizes.<sup>[33]</sup>

Liquid phase methods, such as co-precipitation, microemulsion, and sol-gel synthesis, are the most widely used techniques for synthesizing SPIONs. These techniques employ a bottom-up approach, producing particles in colloidal form. While these methods can yield crystalline and monodisperse particles and offer facile synthesis routes, they often fall short in generating large-scale quantities of nanoparticles.<sup>[32,34]</sup>

In recent years, flame aerosol reactors have garnered interest due to their ability to produce nanoparticles on a large scale. This technique has shown promise in overcoming the limitations of traditional synthesis methods, paving the way for more widespread clinical applications of metal-based nanomaterials. Using the flame spray pyrolysis (FSP) technique is highly efficient for large-scale production, making it suitable for industrial applications. FSP has shown to allow precise control over particle size, composition, and morphology by adjusting flame parameters and precursor solutions.<sup>[35,36]</sup> The high temperatures achieved in the flame ensure the production of highly crystalline and pure nanoparticles, enhancing their magnetic properties.<sup>[37]</sup> Additionally, the process is relatively fast and can produce nanoparticles continuously, which is beneficial for consistent quality and scalability. The versatility of FSP also enables the synthesis of complex nanostructures and composites by simply altering the precursor materials, making it a highly adaptable method for various applications in nanotechnology.

## Bioconjugation of nanoparticles

The potential of SPIONs for biomedical applications is evident. However, to maximize efficacy and minimize off-target effects, precise targeting to specific tissues is essential. Targeting known disease biomarkers with nanoparticles require them to reach their target *via* systemic circulation (if administered systemically) or to cross the intestinal epithelium (if administered orally). On the other hand, local diseases in the GI tract, such as IBD or colon cancer, could directly be targeted through oral delivery, circumventing the need to cross the intestinal epithelium for systemic exposure. This local targeting can be achieved by conjugating the nanoparticles with ligands that bind to receptors uniquely expressed on the surface of intestinal cells.

Bioconjugation of nanoparticles involves attaching biomolecules such as proteins, peptides, DNA, antibodies, or antibody fragments to the surface of nanoparticles to enhance their functionality for biomedical applications. Antibodies, known for their high binding affinity and specificity,<sup>[38]</sup> can be conjugated to nanoparticles, combining their recognition ability with the functional properties of nanoparticles. This synergy makes them highly promising for targeted biomedical applications.

Conjugation strategies for attaching ligands onto the nanoparticle surfaces are mainly categorized into physical adsorption and covalent binding. Covalent bonds are advantageous because they can prevent antibody detachment due to changes in pH or competitive displacement by endogenous molecules, such as proteins.<sup>[38,39]</sup> Common covalent linkages include (1) *carbodiimide chemistry*, which facilitates the formation of amide bonds between carboxyl and amine groups using agents like 1-ethyl-3-(3-dimethylaminopropyl)carbodiimide (EDC) or N,N-dicyclohexylcarbodiimide (DCC),<sup>[40–42]</sup> (2) *maleimide chemistry*, which links thiol groups to maleimide-functionalized nanoparticles,<sup>[43–45]</sup> and (3) *click chemistry*, a highly efficient and versatile method that creates stable covalent bonds *via* the copper-catalyzed azide-alkyne cycloaddition (CuAAC) and the strain-promoted azide-alkyne cycloaddition (SPAAC) (Figure 4).<sup>[46–49]</sup>

Antibodies contain antigen-binding regions, therefore, ensuring proper orientation of these ligands on the nanoparticle surface is crucial for successful target recognition and binding. The carbodiimide reaction involves the conjugation of carboxylic acids and amines, which are prevalent in amino acid side chains distributed throughout the antibody structure. Therefore, this reaction fails to offer control over the orientation of antibodies on the particle surface. Similarly, the maleimide reaction lacks control over ligand orientation and may also disrupt the native structure of antibodies, potentially leading to loss of site-selectivity. In contrast, the click reaction presents a distinct advantage over other conjugation strategies by providing precise control over antibody orientation during covalent conjugation. This is achieved by incorporating azide moieties on the heavy chains of an IgG antibody *via* enzymatic modification.<sup>[50]</sup>

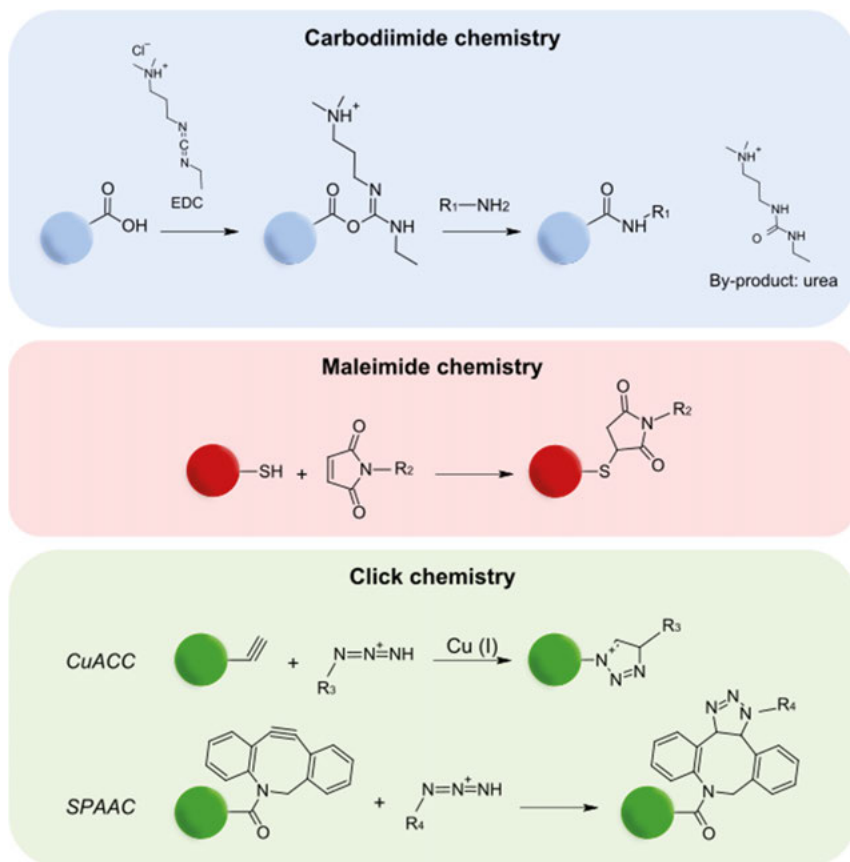


Figure 4. Common reactions for surface modification of nanoparticles.

The advantages of bioconjugation include increased specificity and targeting ability, improved biocompatibility, and the potential for multifunctional platforms that combine therapeutic and diagnostic capabilities (theranostics).

Despite these benefits, several hurdles need to be overcome. Development of reproducible functionalization protocols is challenged by the unique characteristics of nanoparticles, including their strong agglomeration and sedimentation, and adherence to magnets used for mixing of reagents (for magnetic nanoparticles). Additionally, scalable and reproducible production processes need to be developed to meet regulatory standards for clinical applications. Overcoming these obstacles is essential for the successful integration of bioconjugated nanoparticles into medical practice.

## Aim of the thesis

The overall goal of this PhD thesis is to develop a non-invasive diagnostic strategy for IBD utilizing nanoengineering. The project seeks to establish a protocol for the reproducible and scalable synthesis of functionalized SPIONs suitable for MRI detection. This will enhance clinical relevance and applicability. Additionally, the project aims to contribute to the broader objective of creating new non-invasive diagnostic methods for more efficient and targeted diagnosis. The specific objectives are:

- To identify apical plasma membrane biomarkers, present on intestinal epithelial cells in commonly used *in vitro* and *in vivo* preclinical IBD models, and to detect secreted luminal biomarkers *in vivo* (Paper I).
- To develop bioconjugated SPIONs functionalized with ligands targeting the identified biomarkers and assess their subsequent targeting capability *in vitro* (Paper II).
- To develop an experimental procedure to assess the functionalized SPIONs targeting efficacy *in vivo* and their utility as MRI contrast agents for detecting IBD (Paper III).
- To explore the utility of performing *in situ* click chemistry by sequential administration of targeting ligands and SPIONs *in vivo* in the colon to enhance the mucus penetration of particles and increase their targeting capability in colitis-induced mice (Paper III).

# Methods

## Synthesis of iron oxide nanoparticles

### Flame spray pyrolysis

In Papers II and III, flame spray pyrolysis (FSP) was used to synthesize  $\text{SiO}_2$ -coated SPIONs. An enclosed FSP reactor synthesized the core-shell nanoparticles (Figure 5). A 0.34 M Fe precursor solution was prepared by dissolving iron(III) acetylacetonate in a 1:3 mixture of acetonitrile and xylene, stirred for 1 hour, and fed into the FSP nozzle at 5 mL/min, dispersed by 5 L/min  $\text{O}_2$ . The solution spray was ignited by a supporting methane/oxygen flamelet. The FSP reactor was enclosed by a 20 cm quartz glass tube, with a sheath gas flow of 40 L/min  $\text{O}_2$ . Hexamethyldisiloxane vapor was introduced with 0.34 L/min  $\text{N}_2$  through a torus ring with 16 radial equispaced openings and mixed with additional 15 L/min  $\text{N}_2$  gas, resulting in a  $\text{SiO}_2$  content of 23 wt% in the product particles.<sup>[35]</sup> Particles were collected on a glass fiber filter using a vacuum pump.

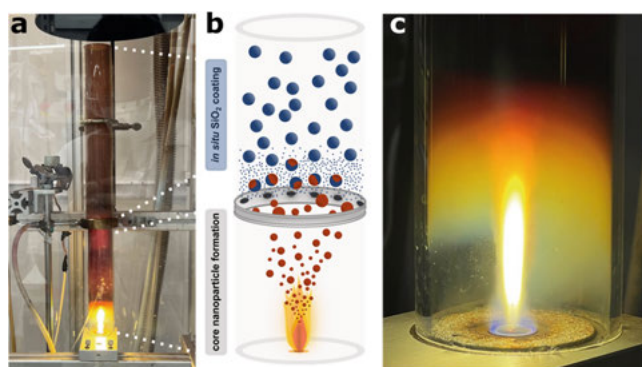


*Figure 5.* Enclosed FSP setup for single-step synthesis of core-shell nanoparticles. (a) The actual flame reactor and (b) schematic illustration of the core nanoparticle formation zone, followed by the swirl injection of the coating precursor, enabling *in situ*  $\text{SiO}_2$  coating of the freshly-made SPIONs. (c) Photograph showing the core nanoparticle formation zone of the reactor with the SPION-producing flame. The flame is supported by the small  $\text{CH}_4/\text{O}_2$  pre-mixed flame (visible with a blue hue). The flame is sheathed with  $\text{O}_2$  provided through the sinter metal plate surrounding the FSP nozzle. The flame is enclosed with a quartz glass tube, to enable the subsequent *in situ* coating of the SPIONs with  $\text{SiO}_2$ .

# Functionalization of nanoparticles

## Silanization

All FSP-made SPIONs produced in Papers II and III were modified with using (3-aminopropyl)triethoxysilane (APTES) as the first functionalization step. This step introduced amines to the particle surface, which is a more nucleophilic moiety compared to the hydroxyl groups of the SiO<sub>2</sub> coated surface. SPIONs were dispersed in dimethylformamide (DMF) (1 mg/mL) by using a Vibra-Cell sonicator (Sonics, Newton, CT, USA) with a 13 mm probe tip operating at 20% amplitude, pulse 10 sec on and 1 sec off, for 3 min. In order to investigate whether the amount of added APTES influences the amount of surface accessible amines available for further conjugation, SPIONs were reacted with 0.6 vol%, 2 vol% or 6 vol% APTES. The reactions were left overnight at 75°C under rotation.

## Synthesis of alkyne-containing linker

In Papers II and III, a short and easily synthesized alkyne-containing linker was prepared by dissolving 6-heptynoic acid (1 equiv) in anhydrous dichloromethane (DCM). N-hydroxysuccinimide (NHS) (2.5 equiv) and 1-(3-dimethylaminopropyl)-3-ethylcarbodiimide hydrochloride (EDC, 1.5 equiv) were added sequentially to the reaction flask. The mixture was stirred overnight at room temperature. The product was obtained after aqueous extraction using saturated NaHCO<sub>3</sub> and ether. The solution was dried over Na<sub>2</sub>SO<sub>4</sub>, concentrated under reduced pressure, and yielded the product as a white/yellow solid (94% yield). The product was used without further purification in subsequent steps.

## Introducing a click-handle

In Paper II, APTES-modified SPIONs were functionalized with alkyne moieties using either a short EDC/NHS-crosslinked linker or a commercially available PEG-linker. The SPIONs were dispersed in dimethylsulfoxide (DMSO) (1 mg/mL) through repetitive ultrasonication rounds in a water bath and cup horn ultrasonicator at 90% amplitude for 1 min, ensuring no aggregates remained. Triethylamine was introduced to the suspension. Either 6-heptynoic acid succinimidyl ester or alkyne-PEG5-N-hydroxysuccinimidyl ester dissolved in DMSO were added to the particle suspension and subjected to further ultrasonication using a probe tip ultrasonicator (20% amplitude, 10 sec pulse on and 1 sec off, 3 min). The reactions were incubated overnight at 50°C with rotation.

To enhance the dispersibility of the alkyne-modified particles, carboxylic acid moieties were introduced to the particle surface in Paper III. Using the

same procedure as previously described, 6-heptynoic acid succinimidyl ester and succinic anhydride were reacted with SPIONs, producing particles with both alkyne and carboxylic acid moieties (Figure 6, product 13).

Additionally, a third type of linker, dibenzocyclooctyne (DBCO)-N-hydroxysuccinimidyl ester (Figure 6, compound 15) was investigated. This diaryl-strained-cyclooctyne enables strain-promoted click chemistry, allowing the SPIONs to bind with antibodies without the need for a copper catalyst.

## Antibody conjugation

In Paper II, antibodies targeting ICAM1 (ab171123, Abcam, Cambridge, UK) were used for SPION conjugation, while in Paper III, antibodies targeting either Icam1 (ab171123, Abcam, Cambridge, UK) or Ceacam1 (ab180789, Abcam, Cambridge, UK) were employed. All antibodies were azide-modified on the Fc-region using Invitrogen™ SiteClick™ Antibody Azido Modification kit (Invitrogen, CA, USA), according to the supplier's instructions.

For both Paper II and III, alkyne-modified SPIONs were dispersed in 1xTris buffer (1 mg/mL) using cup horn (Sonics, Newton, CT, USA) operating at 90% amplitude for 1 min. The sonication was repeated until no aggregates were observed. Sodium ascorbate and CuSO<sub>4</sub> were added to the suspensions. The azide-modified antibodies were transferred to the mixtures and the reactions were left overnight at room temperature under rotation. In Paper II different amounts of antibody was added to the particle suspensions, both in the presence and absence of copper, in order to compare the amount of physisorbed and covalently attached antibodies.

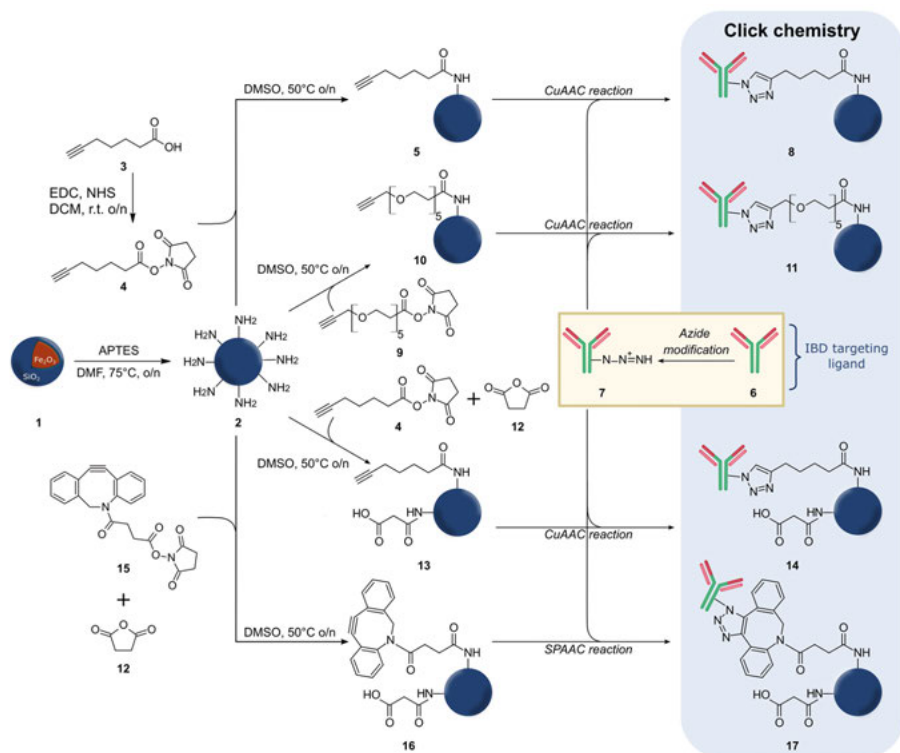


**Figure 6.** Reaction scheme of the attachment of antibody ligands (6) onto SPION (1) surface *via* click chemistry through four different functionalization pathways. Amines were introduced to the SPION surface through silanization reaction using APTES (2). An alkyne-containing linker was synthesized using EDC/NHS crosslinking to yield the NHS-activated carbonyl compound (4). Alkyne moieties were installed onto the nanoparticle surface to yield SPION-linker (5) and SPION-PEG (9). Succinic anhydride (12) was simultaneously added with either the short alkyne-linker (4) or DBCO-N-hydroxysuccinimidyl ester (15) to yield SPION-COOH-linker (13) or SPION-COOH-DBCO (16), respectively. Lastly, alkyne-bearing SPIONs were reacted with azide-modified antibodies (7) to yield the final bioconjugated particles SPION-linker-Ab (8), SPION-PEG-Ab (11) SPION-COOH-linker-Ab (14) and SPION-COOH-DBCO-Ab (17).

## Physicochemical characterization of nanoparticles

After each functionalization step prior to the final antibody-conjugation, all particles were washed by centrifugation (20 000 g, 10 min, 21°C), with the supernatant removed and particles re-dispersed in fresh methanol (MeOH). Particles were dried at 60°C for at least 2 h prior to characterization and further functionalization. The antibody-conjugated SPIONs were washed by magnetic decantation with phosphate-buffered saline (PBS) and either re-suspended in PBS/Tris buffer or dried at 37°C for 2 h prior to characterization.

## X-ray diffraction

In Paper II, the crystalline structure of the FSP-made SiO<sub>2</sub>-coated  $\gamma$ -Fe<sub>2</sub>O<sub>3</sub> nanoparticles was analysed using X-ray diffraction (XRD). Measurements were performed with a D2 Phaser X-ray diffractometer equipped with a LYNXEYE XE-T detector. Cu-K $\alpha$  radiation (wavelength 0.154 nm) was employed at 30.0 kV and 10.0 mA. The XRD pattern was recorded from 20.0° to 80.5° 2 $\theta$  with a step size of 0.01° 2 $\theta$ . Data processing, including background subtraction and baseline smoothing, was conducted using DIFFRAC.EVA software.

## Attenuated total reflectance Fourier-transform Infrared spectroscopy

Nanoparticles in Papers II and III underwent surface functional group analysis using an Attenuated total reflectance Fourier-transform Infrared (ATR-FTIR) spectrometer (Alpha II, Bruker, Germany) with a diamond crystal. After drying at 60°C for 2 hours, measurements were conducted at room temperature with a resolution of 4 cm<sup>-1</sup>, covering the range of 4000-400 cm<sup>-1</sup>. Baseline correction was applied to each spectrum using OPUS software.

## Transmission Light Microscopy

In Paper II, the morphology of pristine SiO<sub>2</sub>-coated SPIONs were studied using transmission light microscopy (TEM). The nanoparticles were suspended in 99.5% ethanol and placed on a Formvar and carbon 300 square mesh copper grid (Delta Microscopies, France). Particle morphology was examined using TEM with a JEM-2100F instrument (Jeol Ltd., Japan), operating at 200 kV with a Schottky-type field emission gun.

## Thermogravimetric analysis

The amount of organic material on the functionalized SPIONs produced in Papers II and III was analysed using a thermogravimetric analyser (TGA) (Discovery, TA Instruments Ind., USA). The experiments were performed under a nitrogen gas flow of 20 mL/min with a heating rate of 10°C/min from room temperature to 900°C. Data was normalized to 120°C, and each experiment was repeated at least three times (n  $\geq$  3).

## Dynamic light scattering

The hydrodynamic diameter of all particles in Papers II and III was determined using dynamic light scattering (DLS) with a Litesizer 500 instrument (Anton-Paar, Austria). Suspensions were diluted to 1 mg/mL in DMF, DMSO, water,

Tris buffer or PBS before measurement. Measurements were conducted in a quartz cuvette.

## Sodium dodecyl-sulphate polyacrylamide gel electrophoresis

To distinguish physisorbed antibodies from covalently attached ones, sodium dodecyl-sulphate polyacrylamide gel electrophoresis (SDS-PAGE) was performed in Paper II. Particles were bioconjugated with ICAM1-targeting antibodies, both in presence and absence of copper catalyst. Bioconjugated particles dispersed in PBS (1 mg/mL) were diluted in SDS buffer, consisting of Tris-Cl, glycerol, SDS and bromophenol. The samples were heated to 95°C for five minutes. A standard curve was made to quantify the physisorbed proteins on the particles, using the azide-modified antibody. Proteins were separated at 4°C using pre-casted gels (Bio-Rad Laboratories AB, CA, USA) with an applied voltage of 200 V. The gels were analysed using GelDoc Go Gel imaging system (Bio-Rad Laboratories AB, CA, USA).

## Quantification of functional groups

### Surface accessible amines

In Paper II, the amine groups on APTES-modified SPIONs were quantified by reacting the particles with 9-fluorenylmethoxycarbonyl chloride (Fmoc-Cl). Fmoc groups attached to free amines were then cleaved with piperidine, producing a UV-active dibenzofulvene-piperidine adduct. This adduct was quantified using UV-Vis spectroscopy at 301 nm, comparing the absorbance to a calibration curve prepared with Fmoc-Valine-OH.

### Terminal alkynes on SPION surface

To quantify the number of alkynes moieties on the linker- and PEG-conjugated SPIONs in Paper II, the particles were reacted with fluorophores *via* click chemistry. Alkyne-modified SPIONs were dispersed in DMSO (1 mg/mL) using repetitive rounds of ultrasonication using water bath and cup horn ultrasonicator operating at 90% amplitude for 1 min, until no aggregates were observed. Sodium ascorbate and CuSO<sub>4</sub> were added to each suspension, followed by azide-containing fluorophore with emission/excitation wavelengths at 519/495 nm. The reactions were left in dark overnight at room temperature under rotation. The particles were washed, dried and re-dispersed in DMSO for analysis of fluorescent intensity using Spark plate (Tecan, Austria). A calibration curve was prepared using known concentrations of the fluorophore as standard samples.

## Fluorescent labelling of bioconjugated SPIONs

After the antibody-conjugation step, a fluorophore was clicked on the antibodies to serve two crucial purposes: firstly, to confirm the presence of targeting ligands on the SPIONs, and secondly, to facilitate imaging of the particles to which they are bound. The fluorescent labelling was performed by clicking the antibody-conjugated particles with a dibenzocyclooctyne-functionalized probe (Alexa488 or Alexa647; Invitrogen, CA, USA).

## *In vitro* methods

### *In vitro* IBD model

Human epithelial colorectal adenocarcinoma (Caco-2) cells are commonly used for studying intestinal cell physiology, drug transport and cell permeability.<sup>[51]</sup> Therefore, in Papers I and II, Caco-2 cells (American Type Culture Collection, VA, USA) were cultured and treated to simulate the acute inflammatory state of the intestine *in vitro*.

Caco-2 cells of passage 95-105 were maintained in Dulbecco's modified Eagle's medium (DMEM) containing fetal bovine serum (FBS) and nonessential amino acids (NEAA). The cells were cultured in an incubator at 37°C, 10% CO<sub>2</sub> while maintained in 75 cm<sup>2</sup> tissue culture flasks.<sup>[52]</sup>

The global proteome of inflammation-induced Caco-2 cells was studied in Paper I. For this, Caco-2 cells were seeded on Transwell polycarbonate filters (Corning, NY, USA; diameter 12 mm, pore size 0.4 μm) and maintained in DMEM supplemented with FBS, NEAA, penicillin and streptomycin. The cells were maintained on filters for 22 days to reach fully differentiated and confluent cell monolayers. The cells were then subjected to either apical exposure of 1% w/v dextran sulphate sodium (DSS),<sup>[53]</sup> or basolateral exposure of a mixture of cytokines, such as tumor necrosis factor (TNF)-α, interleukin (IL)-1β, lipopolysaccharides (LPS) and interferon (IFN)-γ in culture medium.<sup>[54]</sup> The latter will be referred to as TNF-α mixture. The cells were exposed to the inflammatory inducing agents for 24 h. After exposure, the filters were washed with phosphate-buffered saline (PBS) and then excised and prepared for proteomics analysis (Figure 7).

### Cell viability after exposure to functionalized SPIONs

Studying the cell viability after SPION exposure is important for evaluating their biocompatibility and potential use for biomedical applications. Undifferentiated Caco-2 cells, more sensitive to toxicity than their differentiated counterparts, were used for cell viability tests. In Paper II, four types of SPIONs were investigated: bare γ-Fe<sub>2</sub>O<sub>3</sub>, SiO<sub>2</sub>-coated γ-Fe<sub>2</sub>O<sub>3</sub> (SPION), SPION-linker-Ab, and SPION-PEG-Ab particles. Caco-2 cells were plated in black

96-well plates ( $5 \times 10^4$  cells per well) and allowed to attach for 24 hours. Particle suspensions were then added in six replicates per treatment and incubated for 24 hours. Positive controls used 0.22% SDS, and the culture medium served as a negative control. Cell viability was assessed using the CellTiter-Glo Luminescent assay.

### Binding efficacy of bioconjugated SPIONs *in vitro*

The binding efficacy of the bioconjugated SPIONs was assessed using inflammation-induced Caco-2 cells grown on Transwell filters. To prevent nanoparticle sedimentation and false positive results, in Paper II, Caco-2 cells were seeded on the underside of Transwell filters until fully differentiated. Inflammation was induced with the previously described TNF- $\alpha$  mixture. Cells were seeded on polycarbonate filters (Corning, NY, USA; diameter 6.5 mm, pore size 0.4  $\mu\text{m}$ ) at  $0.15 \times 10^6$  cells/filter and maintained in DMEM supplemented with FBS, NEAA, penicillin and streptomycin.

### Staining of filter-grown Caco-2 cells

In Paper II, Caco-2 cells were grown on the bottom side of Transwell filters until fully differentiated and confluent. The cells were then treated with inflammatory agents and exposed to SPIONs as previously described. After washing the filters with HBSS for 5 min, 37°C at 300 rpm, filters were fixed in 4% paraformaldehyde for 15 min at room temperature, followed by permeabilization with 0.2% Triton-X-100 for 15 min at room temperature. Each filter was rinsed with PBS three times and then incubated in a 3% BSA solution in PBS with 0.1% Tween 20 (PBST) for 1 h at room temperature to block non-specific binding. The filters were then incubated with primary monoclonal anti-ICAM1 antibody for 1 h in darkness at room temperature. Filters were washed with PBST for 5 min, three times. Filters were then incubated with secondary antibody (Alexa Fluor 555) for 1 h in darkness at room temperature. Filters were washed with PBST for 5 min, three times and then nuclei were stained with Hoechst for 15 min in darkness at room temperature. Filters were washed with PBS for 5 min, three times.

## *In vivo* methods

### *In vivo* IBD model

All animal experiments were approved by the Swedish Laboratory Animal Ethical Committee in Uppsala (animal experiment number C6/16 for Paper I and 5.8.18-03569/2021 for Paper II) and were conducted in accordance with guidelines of the Swedish National Board for Laboratory Animals.

Animal experiments were conducted in Papers I and III, both involving the induction of acute colitis in mice. The *in vivo* IBD model used in these papers included mice treated with 3% (w/v) DSS (molecular weight ~40 kDa) in their drinking water for one week, resulting in the onset of acute colitis.<sup>[55]</sup> All animals were kept under standardized conditions at 21–22 °C with a 12-hour light/dark cycle. The colitis progression was evaluated for each DSS-treated mouse by daily assessment of clinical parameters (weight loss, stool consistency, and blood content). It was reported as a disease activity index (DAI) score with a minimum of 0 and maximum of 4.<sup>[56]</sup> At the end of the experiment, the mice were euthanized by isoflurane inhalation followed by cervical dislocation.

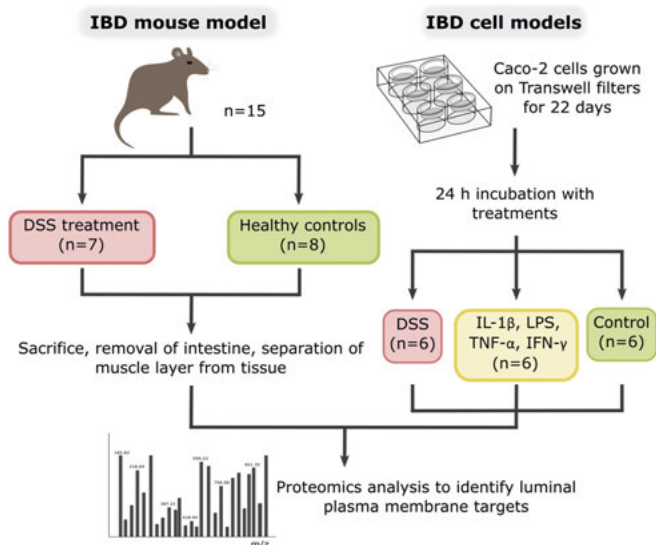


*Figure 7.* Workflow for global proteomics of inflammatory mouse and Caco-2 cell models. Mice (WT, male, C57BL6/J) were treated with DSS in their drinking water for seven days. Intestinal biopsies were collected from ileum, proximal and distal colon. Filter-grown Caco-2 cells were treated with DSS or a mixture of inflammatory agents.

## Administration of bioconjugated SPIONs *in vivo*

Assessing the targeting efficacy of bioconjugated particles *in vivo* typically involves either systemic administration or gavage feeding, with the latter being more relevant for oral delivery applications like detecting IBD in the colon. However, gavage feeding poses challenges due to the stomach's harsh conditions, such as low pH and degrading enzymes, which can compromise the integrity and specificity of the targeting antibodies on the SPIONs, potentially impairing their recognition capabilities. In Paper III, a novel method for rectal administration of bioconjugated SPIONs was developed, bypassing the upper GI tract's harsh conditions (Figure 8). Sedated healthy and colitis-induced transgenic mice expressing cyan fluorescent protein (CFP)-tagged E-cadherin underwent a surgical procedure involving a proximal colon incision and rectal flushing to empty luminal content. Suspensions of fluorescently labelled SPIONs (1 mg/mL) were introduced into the colon and secured with sutures. After 30 minutes of incubation, the tissue was rinsed, excised, mounted inside-out on a holder pin, and placed in a custom 3D-printed chamber for fixation. The tissues were analysed using scanning laser confocal microscopy and MRI imaging. This approach enabled detailed visualization of SPION localization on the luminal side of the colon.

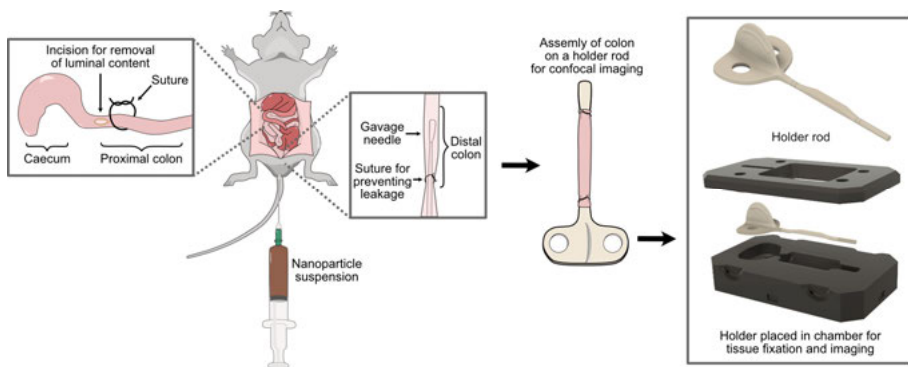


Figure 8. Schematic illustration of *in vivo* incubation and subsequent tissue preparation for *ex vivo* imaging of targeted SPIONs in mice.

## Tissue biopsy sampling for proteomics

Tissue sampling for the proteomic analysis conducted in Paper I included male C57BL6/J mice (Taconic M&B, Ry, Denmark and Charles River, Sulzfeld, Germany), weighing 20-35 g before DSS treatment. Fifteen mice were randomly divided into two groups: control ( $n = 8$ ) and DSS-treated ( $n = 7$ ) (Figure 7).

Intestinal sections of the ileum and colon were removed, placed in oxygenated Krebs solution, and rinsed to remove stool. A midline incision was made along the intestine, and the tissues were pinned luminal side down on a Sylgard-lined Petri dish. The muscle layer was carefully removed, and the entire

ileum was snap-frozen in liquid nitrogen. The large intestine was cut into proximal and distal segments before also being snap-frozen. All tissue samples were stored at  $-80^{\circ}\text{C}$  until further analysis.

## Global proteomics analysis

In Paper I, cell- and animal samples were prepared for global proteomics using a bottom-up approach. Mouse ileum, proximal and distal colon samples were homogenized in lysis buffer containing high concentration sodium dodecyl sulphate (SDS), dithiothreitol (DTT), and Tris/HCl, pH 7.8. The Caco-2 cells were lysed directly with the lysis buffer. Proteins were denatured at  $95^{\circ}\text{C}$  and DNA were sheared with a rod sonicator. Samples were prepared for proteomics analysis using filter-aided sample preparation (MED-FASP) protocol, using LysC and trypsin.<sup>[57]</sup> Protein and peptide amounts were determined based on tryptophan fluorescence.<sup>[58]</sup>

The peptides were subjected to LC-MS/MS-based global, label-free, proteomics. The peptide mixtures were ionized with electrospray in positive mode and analysed on a Q Exactive HF mass spectrometer using a data-dependent mode. The top 15 most abundant isotope patterns were selected and fragmented by higher-energy collisional dissociation. The resulting tandem mass spectrometric scans were obtained at 15,000 resolution.

MS data were processed with MaxQuant (version 1.6.10.43),<sup>[59]</sup> where identifying proteins by searching peptide data against mouse (UP000000589) or human (UP000005640) UniProtKB databases. Spectral raw intensities were normalized using variance stabilization and used to calculate protein concentrations with the Total Protein Approach.<sup>[60]</sup>

## Data Analysis and Bioinformatics

The global proteomics data in Paper I was refined and analysed to identify significant proteins following the procedure outlined in Figure 9. Only proteins identified with at least two unique + razor peptides (peptides shared between protein groups) were considered. Differentially expressed proteins in treated vs. control samples were identified using *limma* in R/ Bioconductor,<sup>[61]</sup> focusing on those with a fold change  $> 2$  and p-value  $< 0.05$ . Functional annotation clustering was performed using the clusterProfiler package in R.<sup>[62]</sup> Only proteins without missing values in any sample were selected (Fig. 1b, step 2). Next, proteins with a significant fold change (p-values  $< 0.05$  from *limma*-analysis; Fig. 1b, step 3) in treated versus healthy controls were chosen for further analysis. Since *limma*-analysis does not account for missing values, proteins upregulated in treated mice and cells but absent in controls were manually added to the selection (Fig. 1b, step 4). Significant fold changes for these

proteins were calculated using a t-test corrected for multiple comparisons with the Holm-Sidak method in GraphPad Prism (version 8.4.0). For the mouse proteome, proteins with higher concentrations in the treated colon than in the healthy ileum were chosen (Fig. 1b, step 5), as inflammation in the mouse model primarily occurs in the colon. Therefore, an imaging probe should target the colon and not bind prematurely in the small intestine. Subsequently, upregulated proteins with a concentration fold change (geometric mean concentration treated/control)  $\geq 1.5$  (Fig. 1b, step 6) in proximal and distal colon were selected. Finally, to ensure sufficient protein concentration for targeting, only proteins with a geometric mean concentration  $\geq 0.5$  fmol/ $\mu$ g total protein (Fig. 1b, step 7) were considered.

The subcellular location of these proteins was determined based on their UniProt annotation.

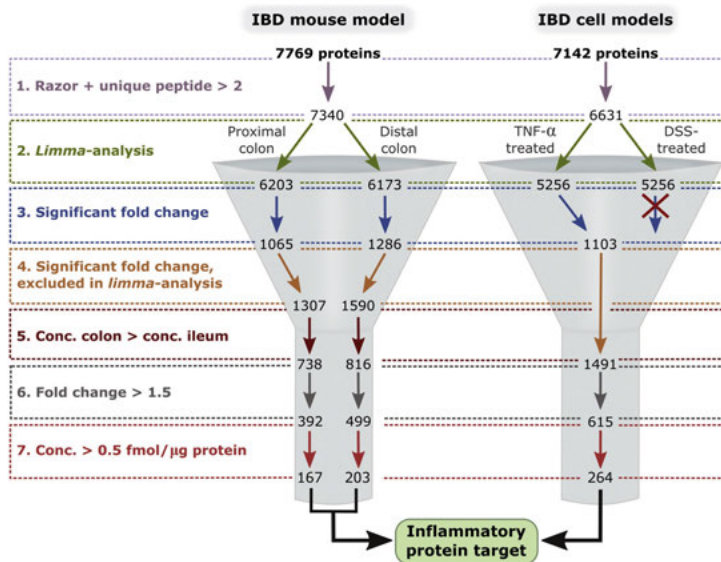


*Figure 9.* Selection criteria to process global proteomics data from intestinal segments from inflamed mice and TNF- $\alpha$  treated Caco-2 cells. Proteins identified as apically expressed on the plasma membrane (according to UniProt annotation) were further investigated for their potential as inflammatory targets for oral delivery in the studied *in vivo* and *in vitro* IBD models.

## Analysis of *in vitro* and *in vivo* samples

### Immunohistochemical analysis

In Paper I, immunohistochemical analysis was conducted to verify the subcellular location of proteins identified through global proteomics. Twelve mice were divided into control (n = 6) and DSS-treated (n = 6) groups. Colon tissues were processed using the Swiss-roll technique, fixed in 4% formalin, embedded in histowax, and sectioned. The sections were stained with specific antibodies against annexin A1, CEACAM1, ICAM1, and transglutaminase 2. Staining procedures included antigen retrieval, application of primary and secondary antibodies, counterstaining, and mounting. The stained sections were imaged with light microscopy using the Axio Scan.Z1 system.

### Inductively coupled plasma optical emission spectroscopy

In Paper II and III, inductively coupled plasma optical emission (ICP-OES) spectroscopy was used to quantify the amount of Fe present in cells and tissues after exposure to bioconjugated SPIONs.

In Paper II, Caco-2 cells grown on the bottom side of Transwell filters were subjected to anti-ICAM1-conjugated SPIONs, followed by washing, excision and dissolution in 1M NaOH at 60°C overnight. The mixtures were centrifuged and supernatant was discarded. Samples were resuspended in 12M HCl and heated to 80°C for 1 hour. In paper III, healthy and DSS-treated mice were exposed to SPIONs functionalized with either anti-Icam1 or anti-Ceacam1 for 30 min. The tissues were rinsed with PBS, excised, segmented into proximal and distal colon, and snap frozen in liquid nitrogen. The samples were stored at -80°C. Tissues were homogenized in 1M NaOH, then incubated at 60°C overnight. Next, 12M HCl was added and samples were heated to 80°C for 1 hour.

The samples were diluted with milliQ water containing 5% HNO<sub>3</sub>, filtered, and measured using the Avio 200 Scott/Cross-Flow Configuration for ICP measurements. A 4-point calibration curve was created with Fe concentrations of 0, 0.1, 0.25, and 0.5 ppm.

### Confocal microscopy

Confocal laser microscopy in Paper II and III was used to image fluorescently labelled particles after exposure to inflammation-induced Caco-2 cells and healthy and DSS-treated mice. In Paper II, images were acquired using an inverted laser scanning confocal microscope from Zeiss LSM 780 with a 63× objective (Zeiss, Oberkochen, Germany). In Paper III, the chamber containing the holders with the tissues were mounted on a Scientifica MMBP stage connected to a Leica SP8 point-scanning confocal microscope with a Leica HC

Fluotar L 25x/0.95-W VISIR objective (Leica Microsystems, Wetzlar, Germany).

## Magnetic resonance imaging

Fixed tissues used for confocal microscopy were also scanned with MRI (9.4 T, BioSpec®, Bruker, Germany) The tissues were mounted inside-out on plastic holder rods (Figure 8), which in turn were assembled on a 3D-printed holder. The assembly was immersed in PBS within a 15-mL Falcon tube and secured against the receiver coil with a sponge. The receiver coil housing was maintained at 25°C.

The scan procedure included tuning and matching the coil elements, frequency calibration, power calibration, and first order shimming, followed by an overview 3D-Fast Low Angle Shot (Flash) scan. After mapping the static magnetic field and adjusting the shims, the tissues were imaged with a multi-gradient echo (mge3d) sequence (field of view 15.36x15.36x15.36 mm<sup>3</sup>, flip angle 9°, repetition time 70 ms, time to first echo 2.681 ms, six echoes separated by 4.9 ms, matrix size 256x256x256, voxel size 60 µm, scan time 1 h 54 min 41 sec). This sequence was repeated six times to monitor potential drift.

Images were processed in Napari software using a filter that inverts the signal (from black to white) and homogenizes the background: Black top-hat (n-SimpleITK), Radius (XYZ): 10

# Results and discussion

## Proteomics-based identification of targets for *in situ* targeting of IBD (Paper I)

Targeting of diagnostic or therapeutic agents to the inflamed intestine necessitates biomarkers that are overexpressed during inflammation compared to the healthy state. To identify such preclinical IBD biomarkers, global proteomic analysis was used to investigate commonly used *in vitro* and *in vivo* inflammatory models. The focus was particularly on discovering biomarkers suitable for *in situ* targeting, including apical plasma membrane biomarkers on intestinal cells both *in vitro* and *in vivo*, and secreted biomarkers *in vivo*. The findings show promise as preclinically relevant targets for developing diagnostic imaging probes and facilitate their study across various experimental IBD model.

### Global proteomics analysis of *in vivo* IBD model

The global proteomics analysis quantified 7340 proteins across ileum, proximal, and distal colon samples. Principal component analysis (PCA) revealed that DSS treatment had a minimal impact on the protein concentrations in the ileum (Figure 10a). In contrast, DSS treatment significantly affected the proximal and distal colon, with 22% and 25% variability attributed to DSS treatment, respectively (Figure 10a). *limma*-analysis revealed significant changes in 128 proteins in the ileum, 257 in the proximal colon, and 437 in the distal colon after DSS treatment (Figure 10b). A correlation (Pearson's  $r = 0.55$ ) was found in protein concentration changes between the proximal and distal colon of treated and control mice, suggesting both segments were similarly affected by DSS treatment (Figure 10c).

Furthermore, functional annotation clustering indicated that the altered protein concentrations in the colon were linked to inflammatory responses (Figure 10d). No significant biological process enrichment was found for the affected proteins in the ileum, highlighting the lower impact of DSS treatment on the ileum compared to the colon.

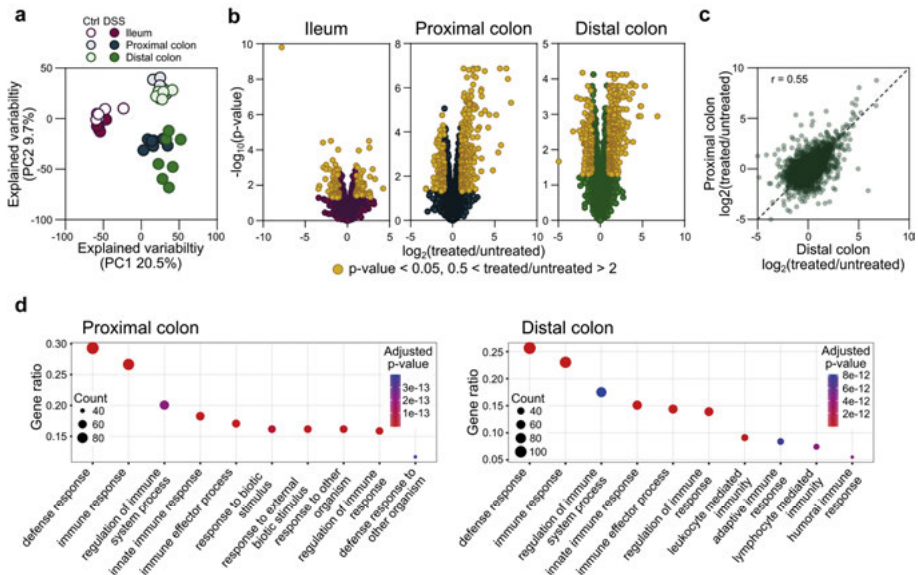


**Figure 10.** Proteomics analysis of ileum, proximal, and distal colon samples from healthy and DSS-treated mice. (a) PCA of protein concentrations. (b) Protein concentration fold change vs. p-values from *limma*-analysis. (c) Correlation of protein concentration fold change between DSS-treated and healthy mice in distal and proximal colon. (d) Enriched biological processes from significantly changed proteins in proximal and distal colon of DSS-treated mice.

## Global proteomics analysis of *in vitro* IBD model

In the Caco-2 cell model, 6631 proteins were quantified, with the most significant changes observed after TNF- $\alpha$  treatment (Figure 11a). PCA revealed that the TNF- $\alpha$  treatment affected 465 proteins, accounting for 25% of the variability (Figure 11a, b). These proteins were involved in defence and cytokine responses, similar to those in DSS-treated mice (Figure 11c). In contrast, DSS treatment altered only 105 proteins in Caco-2 cells, with no enriched functional clusters. Therefore, further analysis was performed using data from only TNF- $\alpha$  treated cells for luminal protein targets.

The differential responses observed between DSS-treated mice and Caco-2 cell cultures can be attributed to the mechanism of action of DSS. While the precise mechanism by which DSS induces intestinal inflammation *in vivo* remains incompletely understood, it is suggested that DSS disrupts the intestinal mucus layer, exposing the epithelium to luminal microbiota.<sup>[63]</sup> This exposure triggers the production of pro-inflammatory substances and recruitment of immune cells, ultimately leading to inflammation. These crucial processes, involving microbiota interaction and immune response, are absent in DSS-treated Caco-2 cell cultures, which lack microbiota, blood flow, and an immune system. DSS has been used in literature as an inflammatory inducing

agent because it can directly impact cell function, demonstrated in studies focusing on cytotoxicity, monolayer integrity, and the release of pro-inflammatory cytokines.<sup>[64,65]</sup> However, for a more accurate replication of the protein expression observed in an inflamed state *in vivo*, TNF- $\alpha$  treatment of Caco-2 cells proves more suitable. This treatment induces an inflammatory response similar to that observed in DSS-treated mice (Figures 9d and 10c).

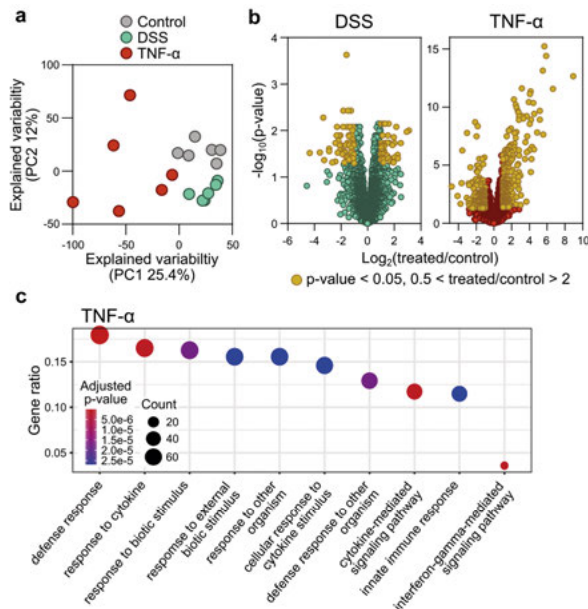


Figure 11. Proteomics analysis of control, DSS, and TNF- $\alpha$  treated Caco-2 cells. (a) PCA of protein concentrations. (b) Protein concentration fold change vs. p-values from *limma*-analysis. (c) Enriched biological processes from significantly changed proteins in TNF- $\alpha$  treated Caco-2 cells.

## Identification of inflammatory biomarkers

The selection process depicted in Figure 9 aimed to identify inflammatory biomarkers in the experimental IBD models. This approach yielded 167 and 203 protein targets in the proximal and distal colon of DSS-treated mice, respectively (Figure 9, step 7). In Caco-2 cells, 264 targets were identified following TNF- $\alpha$  treatment (Figure 9, step 7). Ultimately, proteins that met the criteria across steps 1–7 and that were reported to be *i)* plasma membrane-bound proteins on the apical side of epithelial cells, or *ii)* secreted proteins in the lumen based on UniProt annotations, were selected for further investigation as potential targets for *in situ* applications.

Proteins common in both mouse and cell models are promising candidates for developing diagnostic agents that bridge *in vitro* and *in vivo* models

effectively. In Paper I, four proteins were found to be upregulated during inflammation in both IBD models: Tgm2/TGM2, Icam1/ICAM1, Ceacam1/CEACAM1, and Anxa1/ANXA1 (Table 1). Selection criteria based on fold change and protein concentration were not uniformly met across Caco-2 cells and colon segments, but these proteins were included if criteria were met in at least one sample type.

Icam1/ICAM1 showed the highest upregulation (48-fold) in the Caco-2 cells, while in the distal colon, it exhibited a moderate increase (1.3-fold) and a decrease in the proximal colon (0.7-fold) (Table 1).

Tgm2/TGM2 and Ceacam1/CEACAM1 met selection criteria in both Caco-2 cells (3.5 and 3.6-fold, respectively) and the distal colon (2.4 and 1.6-fold, respectively), with stronger upregulation observed in the distal colon compared to the proximal (1.3 and 1.2-fold, respectively) (Table 1).

Anxa1/ANXA1 had a higher fold change in the proximal colon (1.8-fold) than in the distal colon (1.4-fold) and showed upregulation in Caco-2 cells (2.3-fold), although at a relatively low total protein concentration (geometric mean < 0.5 fmol/ $\mu$ g even after TNF- $\alpha$  treatment) (Table 1).

Immunohistochemistry confirmed the expression of Tgm2, Icam1, Ceacam1, and Anxa1 in inflamed and healthy mouse tissues, consistent with proteomics findings (Figure 12). Anxa1 exhibited moderate expression along intact epithelial cells in the distal colon but was absent in severely inflamed areas. Ceacam1 was prominently expressed on epithelial cell surfaces in both colon regions. Icam1 showed high expression in heavily inflamed regions and Tgm2 in the deeper layers near inflamed regions of the intestine.

**Table 1.** Concentrations of apical, cell membrane proteins in Caco-2 cells and inflamed intestinal segments in mice were measured in fmoI/ $\mu$ g protein. Data is presented as geometric mean values. Non-significant changes are italicized.

Gene name	Caco-2		Proximal colon				Distal colon				Ileum		Comments
	Fold change	Conc. TNF- $\alpha$ treated	Conc. control	Fold change	Conc. treated	Conc. healthy	Fold change	Conc. treated	Conc. healthy	Conc. treated	Conc. healthy		
												Conc. healthy	
<b>Anxa1/ ANXA1</b>	2.3	0.4	0.2	1.8	29.7	16.7	1.4	41.7	31.8	8.6	<ul style="list-style-type: none"> <li>• Annexin A1</li> <li>• Secreted in intestinal mucosal tissues during inflammation</li> <li>• Release of extracellular vesicles containing annexin A1 from epithelial cells promote mucosal wound repair<sup>[66,67]</sup></li> </ul>		
<b>Ceacam1/ CEA- CAM1</b>	3.6	4.9	1.4	1.2	3.0	2.4	1.6	2.6	1.7	1.9	<ul style="list-style-type: none"> <li>• Carcinoembryonic antigen-related cell adhesion molecule 5</li> <li>• Overexpressed on surface of colonic ECs in Crohn's disease<sup>[68]</sup></li> </ul>		
<b>Icam1/ ICAM1</b>	48.0	22.8	0.5	0.7	0.6	0.8	1.3	0.3	0.2	0.2	<ul style="list-style-type: none"> <li>• Intercellular adhesion molecule 1</li> <li>• Upregulated on apical surface of IECs during inflammation<sup>[69,70]</sup></li> </ul>		
<b>Tgm2/ TGM2</b>	3.5	20.2	5.8	1.3	9.4	7.4	2.4	10.6	4.4	9.4	<ul style="list-style-type: none"> <li>• Transglutaminase 2</li> <li>• Apoptosis, cell differentiation, inflammation</li> <li>• Upregulated in mucosal layer in IBD<sup>[71]</sup></li> </ul>		

**Table 2.** Extracellularly located proteins in inflamed intestinal segments of mice. Protein concentrations (fmol/ $\mu$ g protein) were calculated with the Total Protein Approach and are shown as geometric mean values. Fold change is protein concentration in treated/untreated. The listed proteins are sorted with descending fold change in the distal colon.

Gene name	Proximal colon			Distal colon			Ileum		Comments
	Fold change	Conc. treated	Conc. healthy	Fold change	Conc. treated	Conc. healthy	Fold change	Conc. healthy	
<b>Mpo</b>	76.5	1.9	0.02	105.5	1.1	0.01	0.09		<ul style="list-style-type: none"> <li>• Myeloperoxidase</li> <li>• Released from neutrophils and macrophages, exhibits antibacterial effects</li> <li>• Increased levels in feces correlate to disease activity in IBD patients<sup>[72]</sup></li> </ul>
<b>S100a8</b>	265.2	6.4	0.02	33.2	1.6	0.1	0.3		<ul style="list-style-type: none"> <li>• S100a9 and S100a8: heterodimer calprotectin</li> </ul>
<b>S100a9</b>	118.5	31.5	0.3	28.0	11.8	0.4	1.4		<ul style="list-style-type: none"> <li>• Secreted from immune cells during inflammation</li> <li>• Used as feces marker for IBD<sup>[73,74]</sup></li> </ul>
<b>Ltf</b>	91.7	2.8	0.03	20.8	0.9	0.04	1.3		<ul style="list-style-type: none"> <li>• Lactoferrin</li> <li>• Secreted by neutrophils, exhibits antimicrobial effect</li> <li>• Ltf in feces correlates with severity of GIT inflammation<sup>[75]</sup></li> </ul>
<b>Epx</b>	7.6	4.6	0.6	12.7	3.4	0.3	1.4		<ul style="list-style-type: none"> <li>• Eosinophil protein X</li> <li>• Released by activated eosinophils, exhibits cytotoxic effects</li> <li>• Elevated concentrations in feces of IBD patients<sup>[76]</sup></li> </ul>

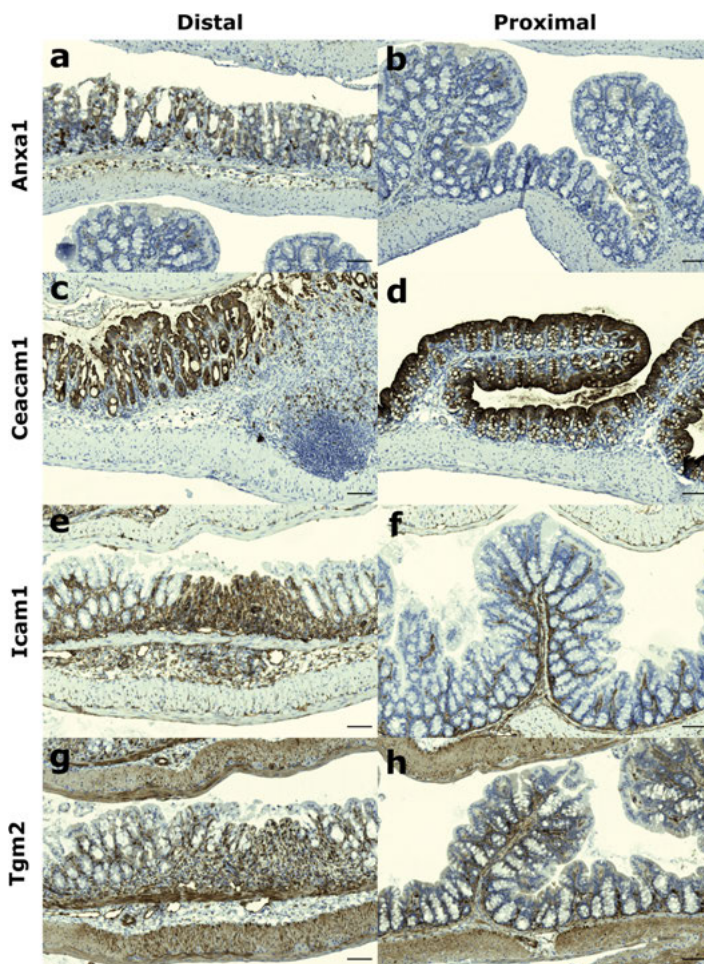


Figure 12. Immunohistochemical staining of protein targets in distal (a-g) and proximal colon sections (e-h) of DSS-treated mice. (scale bar: 20  $\mu$ m)

In addition to these plasma membrane-bound biomarkers, highly upregulated luminal and immune cell-associated proteins were found in the *in vivo* mouse model, such as myeloperoxidase, calprotectin, lactoferrin, and eosinophil peroxidase (Table 2). These biomarkers are clinically used for non-invasive diagnosis using fecal samples from IBD patients. While they serve as useful indicators for diagnosis, their protein concentration does not provide reliable estimations of disease activity, likely due to the tedious sampling process and the time- and temperature-dependent degradation of the biomarkers. Thus, although these proteins do not provide information of disease location, targeting these biomarkers *in situ* could potentially offer quantitative information about IBD disease activity in the GI tract.

## Click chemistry-based bioconjugation of SPIONs (Paper II)

The second paper of this thesis focused on developing MRI active biosensors by functionalizing SPIONs with ligands targeting the biomarkers identified in the first study. The work aimed to establish a detailed protocol for preparing bioconjugated SPIONs for enhanced targeting capabilities *in vitro* based on click chemistry. The findings underscored the importance of systematic nanoparticle surface modification and rigorous characterization in optimizing SPIONs for targeted imaging and therapeutic delivery, paving the way for advancements in precision medicine and diagnostic technologies.

### SPION synthesis and coating

The synthesis of  $\gamma$ -Fe<sub>2</sub>O<sub>3</sub> and *in situ* coating with SiO<sub>2</sub> was performed using FSP. The SiO<sub>2</sub> coating has previously shown to improve the particle dispersibility and biocompatibility in aqueous environments, which is essential for subsequent biomedical use.<sup>[35,36]</sup> The one-step production yielded SiO<sub>2</sub>-coated  $\gamma$ -Fe<sub>2</sub>O<sub>3</sub> nanoparticles, confirmed by TEM and XRD analysis, which showed a crystallite size of 13.5 nm, making them suitable as T2 contrast agents for MRI (Figure 13).<sup>[77]</sup> These particles are referred to as SPIONs.

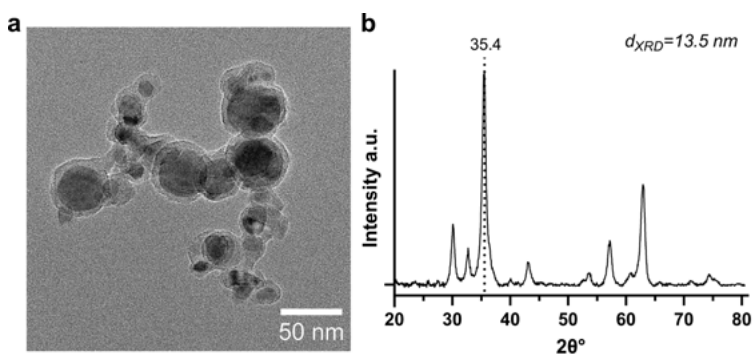


Figure 13. Characterization of flame-made SPIONs. (a) TEM image and (b) XRD pattern of SiO<sub>2</sub> coated  $\gamma$ -Fe<sub>2</sub>O<sub>3</sub>, dashed line corresponds to specific crystallographic (311) plane at  $2\theta = 35.4^\circ$ , indicative of the crystalline structure of  $\gamma$ -Fe<sub>2</sub>O<sub>3</sub>.

### Surface functionalization of SPIONs

#### Silanization to introduce of amines

The choice of solvent is critical for the successful functionalization of nanoparticles, as it impacts their dispersion and prevents agglomeration during conjugation reactions. Therefore, SiO<sub>2</sub>-coated SPIONs were dispersed in various solvents to find a suitable medium for conjugation reactions. Polar

solvents such as methanol (MeOH), ethanol (EtOH), isopropanol (2-PropOH), acetonitrile (ACN), dimethyl sulfoxide (DMSO), and dimethylformamide (DMF) effectively dispersed the particles, while non-polar solvents like dichloromethane (DCM), ether, and toluene caused rapid agglomeration and sedimentation, making them unsuitable for modification reactions (Figure 14a).

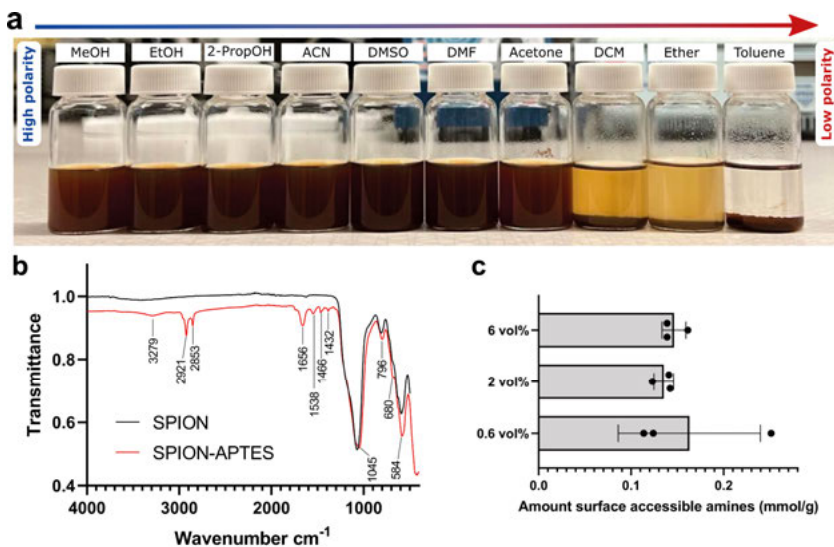
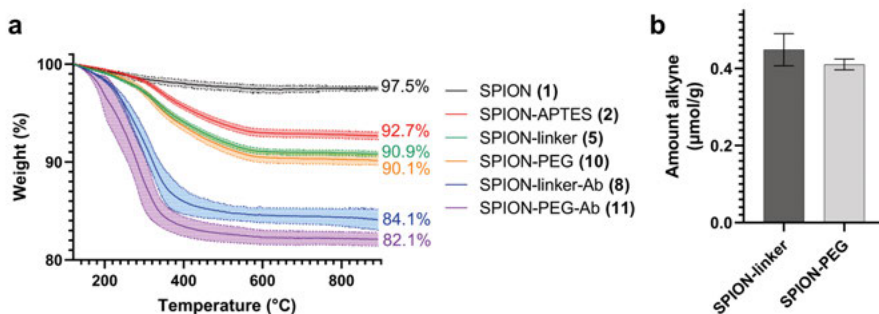


Figure 14. Characterization of APTES-conjugated SPIONs. (a) Suspensions of SPIONs prior to modification in various solvents arranged from high to low polarity (left to right). (b) ATR-FTIR pattern of APTES-modified SPIONs. (c) Fmoc-based quantification of surface accessible amines on APTES-modified SPIONs, values normalized to mmol/g of SPION.

Surface functionalization of SPIONs with organic moieties was initiated with the introduction of terminal amines. A silanization reaction using (3-aminopropyl)triethoxysilane (APTES) in dimethylformamide (DMF) was performed to successfully conjugate the particles, as confirmed by ATR-FTIR (Figure 14b) and TGA (Figure 15a). Various concentrations of APTES was conjugated onto SPIONs to optimize the protocol. Quantification of surface accessible amine groups on APTES-modified SPIONs using Fmoc-Cl and UV-Vis spectroscopy (Figure 14c), revealed that despite different APTES concentrations, the amount of amines on the SPION surface did not vary significantly, suggesting that excess APTES does not necessarily enhance functionalization efficiency. Further functionalization was carried out using 2 vol% APTES in the silanization reaction.

## Instalment of alkyne click handles

Further modification involved installing alkyne handles on the SPION surface via NHS-activated organic linkers (small linker and PEG-linker) for subsequent click chemistry reactions. TGA confirmed successful conjugation of the small linker and PEG, with moderate weight loss reductions (90.9% and 90.1%, respectively) compared to APTES-modified SPIONs (92.7%), indicating successful surface modification (Figure 15a). The quantification of alkynes on the SPION surface was achieved by coupling an azide-containing fluorophore to the alkyne moieties using click chemistry. This method confirmed comparable alkyne densities on SPIONs modified with either linker, crucial for subsequent bioconjugation steps (Figure 15b).



*Figure 15.* Characterization of modified SPIONs. (a) TGA profiles of products obtained after indicated modification step, values normalized to 120°C. (b) Quantification of alkynes on particle surface using fluorescent click-labelling, values normalized to  $\mu\text{mol/g}$  of SPION.

## Antibody conjugation

The final step of the functionalization protocol consisted of the bioconjugation of ICAM1-targeting antibodies (100  $\mu\text{g/mL}$ ) to alkyne-modified SPIONs using CuAAC. Enzymatic modifications to the Fc region of antibodies to introduce azide groups enabled specific and efficient conjugation with SPIONs, yielding SPION-linker-Ab and SPION-PEG-Ab (products 8 and 11, Figure 6). Characterization using TGA (Figure 14a) and fluorescent labelling of conjugated antibodies indicated successful antibody conjugation.

To ensure a thorough comparison, covalently modified SPIONs were evaluated alongside control reactions in the absence of copper. This was conducted to validate the effectiveness of the proposed covalent bioconjugation protocol. TGA profiles revealed that particles conjugated with antibodies in the absence of a copper catalyst exhibited lower weight reduction and greater variability between batches compared to those conjugated in the presence of copper (Figure 16a). Furthermore, SDS-PAGE analysis was conducted to estimate the relative ratios of adsorbed versus covalently attached antibodies on the SPION surface. The results indicated that particles conjugated in the presence of a

copper catalyst had a fraction of non-covalently attached antibodies, but this fraction was smaller compared to particles reacted with antibodies in the absence of copper catalyst (Figure 16b). This suggests that while some non-specific adsorption still occurs, the use of the copper catalyst greatly enhances the efficiency of covalent bonding, thereby reducing the extent of non-covalent antibody attachment. Additionally, increasing the amount of added antibodies to the reaction resulted in a higher amount of non-covalently attached ligands (Figure 16b).

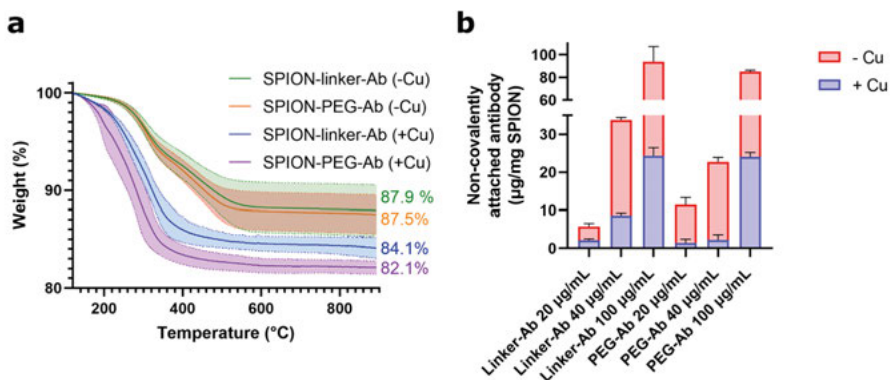


Figure 16. Characterization of antibody conjugation of SPIONs. (a) TGA profiles of antibody-conjugated SPIONs prepared in presence (+ Cu) and absence (- Cu) of copper catalyst. (b) Quantification using SDS-PAGE of non-covalently attached antibodies on particles prepared with 20-100 µg/mL of added antibody (error bars represent standard deviation from technical replicates).

### Targeting capability of bioconjugated SPIONs *in vitro*

The biocompatibility of ICAM-targeted SPIONs was investigated by exposing undifferentiated Caco-2 cells to various concentrations of particle suspensions (100-500 µg/mL) for 24 hours. Cell viability remained high even at the highest particle concentrations tested (Figure 17a). Notably, the SiO<sub>2</sub> coating significantly enhanced particle cytocompatibility, with cells showing 89% viability even at the highest dose, as compared to 69% viability after exposure to uncoated γ-Fe<sub>2</sub>O<sub>3</sub> particles (Figure 17a). SPION-PEG-Ab exposure resulted in a moderate decrease in viability (65%), consistent with literature indicating cytotoxicity of shorter PEG chains.<sup>[78-80]</sup> In contrast, SPION-linker-Ab maintained 85% viability at the highest dose, highlighting its cost-effectiveness, enhanced biocompatibility, and ease of synthesis.

The binding efficacy of both covalently and non-covalently conjugated SPIONs, as well as non-targeted particles was investigated on inflammation-induced Caco-2 cells grown on the bottom surface of Transwell filters. This inverted setup was considered to prevent nanoparticle sedimentation on the cell surface during exposure, which could lead to false positive results. The

inflamed cells were exposed to the different particle formulations for 2 hours and analysed using ICP-OES. The results revealed a significantly higher amount of Fe in cells exposed to SPION-linker-Ab and SPION-PEG-Ab compared to their non-targeted or non-covalently bioconjugated counterparts (Figure 17b, c). This demonstrates that the presence of the targeting ligand, combined with covalent conjugation, significantly enhances the binding specificity and efficacy of the nanoparticles.

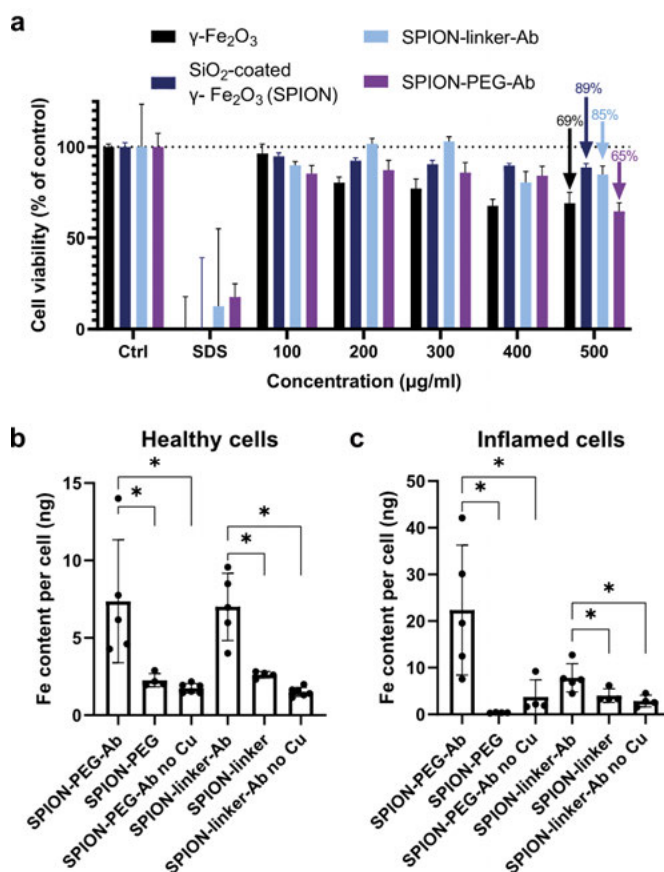
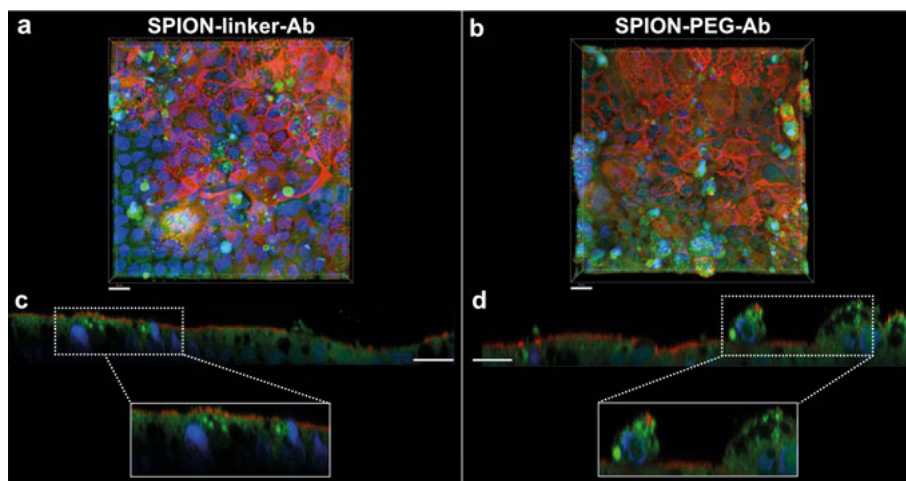


Figure 17. Exposure of functionalized SPIONs to Caco-2 cell monolayers. (a) Cell viability of nondifferentiated Caco-2 cells was assessed after 24-hour exposure to functionalized SPIONs at various concentrations (100-500 µg/mL). Viability was calculated as a percentage of the control (set to 100%). Quantification of Fe in healthy (b) and inflamed (c) cell monolayers after SPION exposure using ICP-OES. Differences were analysed by t-test (\*p < 0.05)

To investigate the interactions of antibody-conjugated particles with epithelial cells, inflammation-induced Caco-2 cell monolayers were grown on the bottom surface of Transwell filters and then exposed to fluorescently tagged

ICAM1-conjugated SPIONs. The filters were visualized using confocal microscopy (Figure 18). Despite an inverted setup to prevent sedimentation-driven interactions, large particle aggregates adhered to the cell surface, indicating active binding (Figure 18a, b). Cross-sectional images showed functionalized SPIONs both apically and internally within the cells, suggesting cellular internalization (Figure 18c, d).



*Figure 18.* Confocal images of differentiated and inflammation-induced Caco-2 cell monolayers cultured in Transwell filters and stained for ICAM1 (red) and nuclei (blue). Overview (a, b) and cross-sectional (c, d) images of inflamed cells exposed to ICAM1-functionalized SPIONs, prepared with 100  $\mu\text{g}/\text{mL}$  antibody (green) (scale bar: 20  $\mu\text{m}$ ).

The fluorophore conjugation to the antibodies both confirmed the presence of targeting ligands on SPIONs and facilitated imaging. A diffuse green signal beneath the cell membrane was observed that could originate from Ab-functionalized SPIONs or desorbed, non-covalently bound antibodies. To study this further, cells were exposed to bioconjugated particles prepared with less antibody (20  $\mu\text{g}/\text{mL}$ , Figure 19a-d). The confocal images were comparable for both antibody concentration used, showing a faint green signal inside the cells in both cases (Figures 17c, d and 18c, d). Additionally, when the cells were exposed to the fluorescently-tagged free antibodies, this diffuse green signal was not observed inside the cells (Figure 19e, f), suggesting that the green signal can be attributed to the cellular internalization of bioconjugated SPIONs.

These observations strongly indicate the internalization of functionalized SPIONs, highlighting their potential for cellular uptake and necessitating further investigation into particle uptake mechanisms.

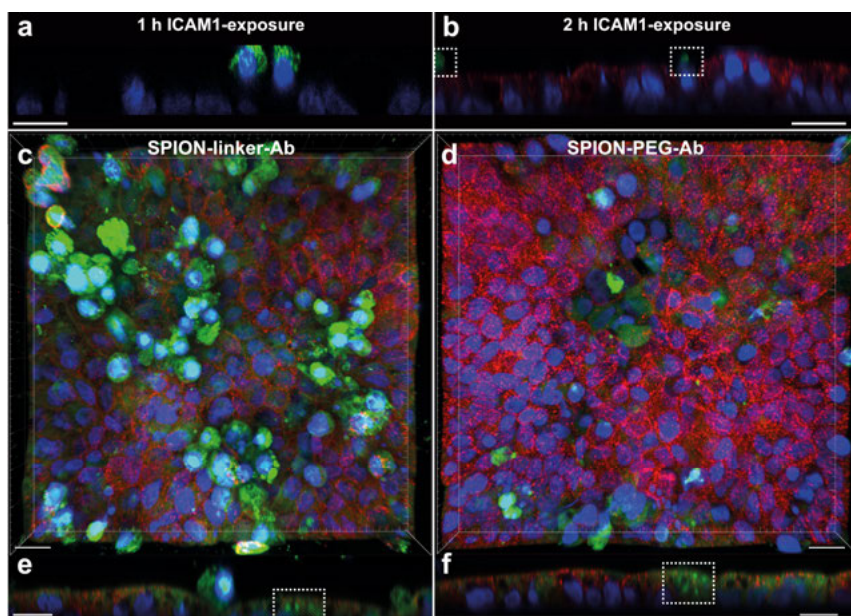


*Figure 19.* Confocal images of inflammation-induced Caco-2 cell monolayers cultured in Transwell filters and stained for ICAM1 (red) and nuclei (blue). (a, b) Overview image of cells exposed to ICAM1-modified SPIONs (green), prepared with 20  $\mu\text{g/mL}$  antibody. Cross-sectional images of cells exposed to fluorescently-tagged free ICAM1 antibodies (green) for 1 (e) and 2 h (f) (scale bar: 20  $\mu\text{m}$ ).

## Targeting efficacy of bioconjugated nanoparticles colitis-induced mice (Paper III)

The third paper of the thesis focused on adapting the functionalization protocol from Paper II to develop nanoparticles targeting inflamed tissue of mice. Furthermore, the study aimed to assess their utility as MRI active biosensors for detecting IBD *in vivo*. The results highlight the potential of bioconjugated SPIONs for targeted imaging and diagnostic applications in inflamed intestinal tissues.

### Introduction of carboxylic acid moieties

The enzymatic modification of azides on the Fc-region of antibodies ensures covalent attachment of the targeting ligand without compromising the binding site, allowing control of the ligand orientation. However, this process may lead to physisorption of antibodies (as evidenced in Paper II, Figure 16b), which can detach in complex environments like the GI tract. Conjugating a fluorophore to these antibodies could cause confusion during imaging. Therefore, it is advantageous to attach the imaging moiety directly to the particle surface to

avoid uncertainties with physisorbed protein dynamics. This was achieved by introducing carboxylic acid moieties to the SPION surface and subsequently attach a fluorophore using carbodiimide chemistry.

Following APTES functionalization of SPIONs, the particles were modified with 6-heptynoic acid succinimidyl ester and succinic anhydride (product 13, Figure 6). Thus, the instalment of alkyne-linker and carboxylic acid proceeded simultaneously.

This process yielded particles with carboxylic acid groups and an alkyne-containing linker, however, experimentally distinguishing between these moieties proved to be challenging. ATR-FTIR confirmed the presence of organic moieties on the SPION surfaces, however, due to overlapping absorbance bands, the presence of both moieties could not be conclusively determined (Figure 20). Similarly, TGA indicated an increase in organic material, but it was not possible to determine whether this consisted of both moieties or just one.

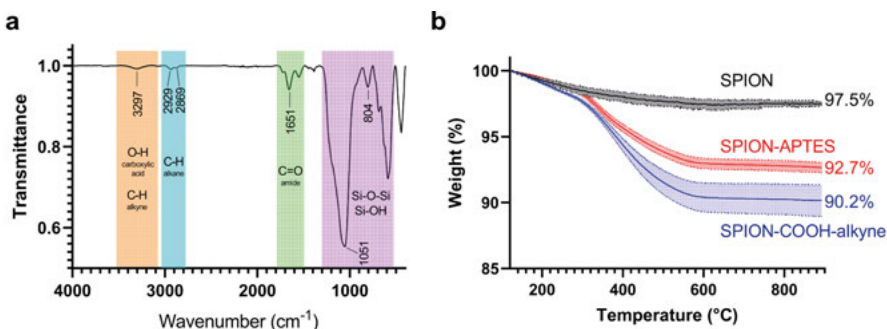


Figure 20. Characterization of SPIONs modified with alkyne-linker and carboxylic acids. (a) ATR-FTIR pattern and (b) TGA profile.

Measurements of hydrodynamic size and zeta potential showed a shift to a negative zeta potential compared to particles only conjugated with the linker, indicating the presence of carboxylic acid groups. The decreased size in alkaline media is likely due to electrostatic repulsions between the negatively charged particles (Table 3).

Another alternative that would circumvent the need for functionalization reactions of SPIONs was explored by modifying particles with a different alkyne-containing linker. Dibenzocyclooctyne (DBCO)-N-hydroxysuccinimidyl ester was conjugated onto the SPION surface with succinic anhydride, producing SPION-COOH-DBCO (product 17, Figure 6). This molecule features an internal alkyne in a strained cyclooctyne structure, allowing for copper-free SPAAC. This reaction eliminates the need for copper as a catalyst, enabling *in vivo* conjugation of particles and targeting antibodies, and circumventing the use of large antibody-nanoparticle conjugates for *in vivo* targeting.

This approach could be beneficial to for the particles to diffuse through the mucus barrier and reach the underlying epithelial cell surface.

**Table 3.** Hydrodynamic size and zeta potential of functionalized SPIONs in Paper II and III.

Functionalized particle	Hydrodynamic size	PDI	Zeta potential	Solvent
SPION	193.7 nm (± 0.83 nm)	21.4 %	-30.3 mV (± 5.6 mV)	DMF
SPION-APTES	146.2 nm (± 1.6 nm)	18.4 %	33.5 mV (± 1.2 mV)	DMSO
SPION-alkyne <sup>a</sup>	> 1 μm	5.1 %	N/A	Tris buffer
SPION-COOH-alkyne	190.4 nm (± 17.4 nm)	25.5 %	-34.1 mV (± 0.4 mV)	Tris buffer
SPION-COOH-alkyne-Ceacam1 <sup>a</sup>	> 1 μm	25.7 %	-15.0 mV	PBS
SPION-COOH-alkyne-Icam1 <sup>a</sup>	> 1 μm	25.0 %	-15.5 mV	PBS
SPION-COOH-DBCO	344.1 nm (± 85.0 nm)	26.6 %	-29.5 mV (± 2.1 mV)	PBS

<sup>a</sup> Measured in one replicate

### Antibody affinity and *in vivo* targeting

The binding affinity of anti-Ceacam1 and anti-Icam1 antibodies was evaluated in the colon of colitis-induced transgenic mice expressing CFP-tagged E-cadherin. The mice were exposed to fluorescently tagged antibodies following the procedure described in Figure 8. This investigation aimed to verify the antibodies' ability to bind effectively to their targets prior to conjugation with SPIONs.

The results demonstrated robust binding of anti-Ceacam1 antibodies, prominently expressed on epithelial cell surfaces and in inflamed mucosal areas lacking epithelium (Figure 21a-c). In contrast, anti-Icam1 antibodies showed minimal expression in confocal images, indicating sparse binding compared to anti-Ceacam1 (Figure 21d-f). Furthermore, this aligns with the findings in Paper I, which showed that the upregulation of Icam1 is significantly less pronounced in healthy tissues compared to inflamed tissues, unlike the upregulation of Ceacam1. The significant difference in protein expression between Ceacam1 and Icam1 underscore the importance of assessing antibody binding capacity early in bioconjugated systems as it offers critical insights for the development of targeted nanoparticles.

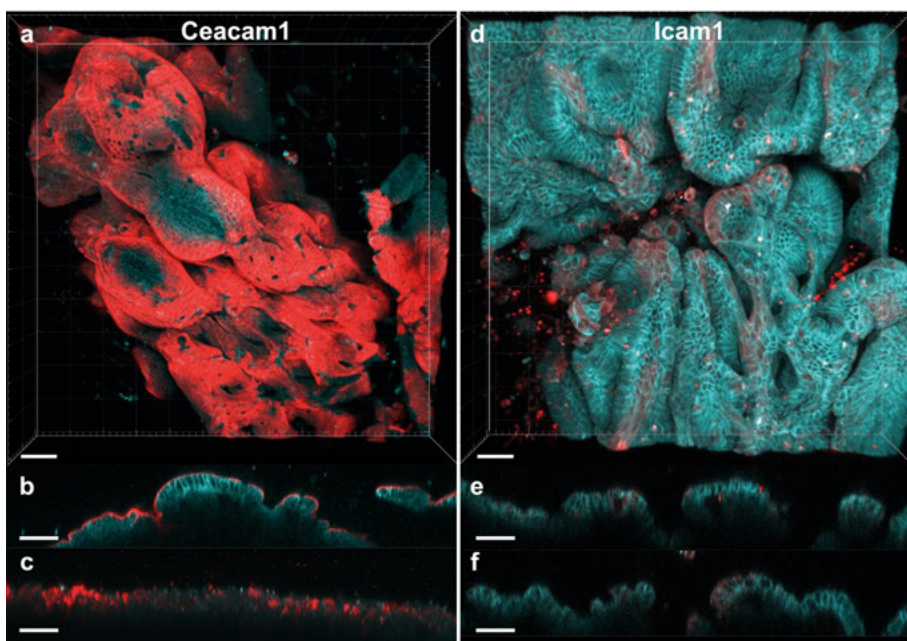


Figure 21. Fluorescence confocal images of colons from colitis-induced CFP transgenic mice depicted epithelial cells (cyan) and fluorescently tagged antibodies (red) targeting Ceacam1 (a-c) and Icam1 (d-f) (scale bars: 50  $\mu\text{m}$ ).

### Targeting efficacy *in vivo*

The established methods for evaluating bioconjugated particle targeting efficacy *in vivo* typically involve systemic administration or gavage feeding,<sup>[81]</sup> particularly for oral delivery applications. For our study focusing on localized detection of IBD in the colon, gavage feeding is most relevant. However, direct administration into the stomach poses challenges due to its harsh environment, potentially compromising the integrity and specificity of the SPION-conjugated antibodies. To overcome these issues, we developed a novel approach involving rectal administration of bioconjugated SPIONs directly into the colon (Figure 8). This method bypasses the harsh upper GI tract conditions, ensuring controlled and targeted delivery to the site of interest. In this approach, mice were sedated, and after a surgical procedure to empty the colon's luminal content, fluorescently labelled bioconjugated SPION suspensions were introduced and incubated within the colon.

### Quantitative assessment of targeting capability of SPIONs

Ceacam1- and Icam1-targeted SPIONs were evaluated for their targeting efficacy after *in vivo* administration. Quantitative assessment involved measuring iron (Fe) concentrations in colonic tissue samples using ICP-OES. To evaluate the baseline Fe levels in colons of mice, controls consisting of mice exposed

to PBS were used. Icam1-conjugated SPIONs showed no increased in binding affinity to inflamed tissue compared to healthy. This is consistent with the proteomics analysis in Paper I, indicating less Icam1 upregulation in healthy versus inflamed tissues (Table 1). It also corresponds well to the low antibody binding observed in colitis-induced mice (Figure 21d-f). In contrast, significantly elevated Fe levels were observed in colons of mice exposed to Ceacam1-conjugated SPIONs compared to both healthy tissue and those exposed to Icam1-conjugated SPIONs (Figure 22). The variability among individuals in disease group is expected, as DSS treatment induces colitis to varying degrees, and each mouse responds differently to the treatment (DAI score ranged between 1.33-4.0). Nonetheless, the significant difference between healthy and diseased mice exposed to Ceacam1-conjugated SPIONs, which was not observed in those exposed to Icam1-conjugated SPIONs, suggests that the Ceacam1-conjugated particles have a specific affinity for targeting diseased tissue. This finding underscores the potential of Ceacam1-conjugated SPIONs for targeted diagnosis and treatment of colitis.

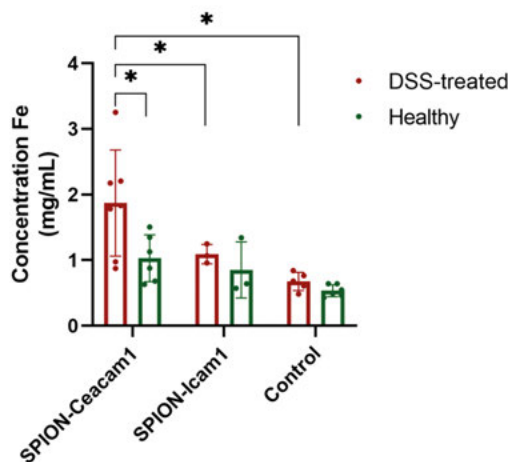


Figure 22. Concentration of Fe in healthy and colitis-induced colons of mice after exposure to bioconjugated SPIONs. Differences were analysed by t-test (\* $p < 0.05$ )

The *in vivo* click conjugation did not reveal any difference between administering the targeting ligand before the particles or administering the particles alone, based on ICP-OES (not shown). Although the DBCO-conjugated particles are significantly smaller than those with pre-attached antibodies, they failed to conjugate with the targeted antibody *in vivo*.

This failure might be due to the presence of carboxylic acid groups on the particles. While these groups enhance particle dispersibility due to their negative charge in alkaline mediums, they might also cause repulsion from the

slightly negatively charged mucus layer. In contrast, antibody-conjugated particles, which have a near-neutral zeta potential and surface charge, performed better at targeting diseased tissue despite being more prone to agglomeration. These findings highlight the complexities of nanoparticle design and the need for careful consideration of surface chemistry to optimize targeting efficiency.

### **Visualization of targeting capability using confocal microscopy**

Fluorescence confocal microscopy was utilized to examine colonic tissues from colitis-induced CFP transgenic mice, revealing distinct morphological changes indicative of inflammation severity. Severely damaged mucosal tissue showed crypt loss and complete de-epithelialization (Figure 23a, b) and areas with moderate damage displayed irregular epithelial structures (Figure 23c, d).

Ceacam1-conjugated SPIONs were found abundantly in severely inflamed regions, adhering prominently to loose connective tissue (Figure 23b). In moderately affected areas, SPIONs were localized near the epithelial layer, likely hindered by the mucus layer from reaching the underlying tissue (Figure 23d). Previous studies have demonstrated depletion of sentinel goblet cells and mucus barrier failure after DSS treatment of mice,<sup>[82,83]</sup> supporting the observation that highly damaged and de-epithelialized mucosa lack the mucosal barrier and thus interfere less with SPION binding to the tissue. In areas with a functioning mucus barrier, large particle agglomerates were observed to be entrapped in the mucus (Figure 23e, f). Thus, the severity of inflammation influenced the mucus layer's protective function, which in turn appeared to affect nanoparticle distribution.

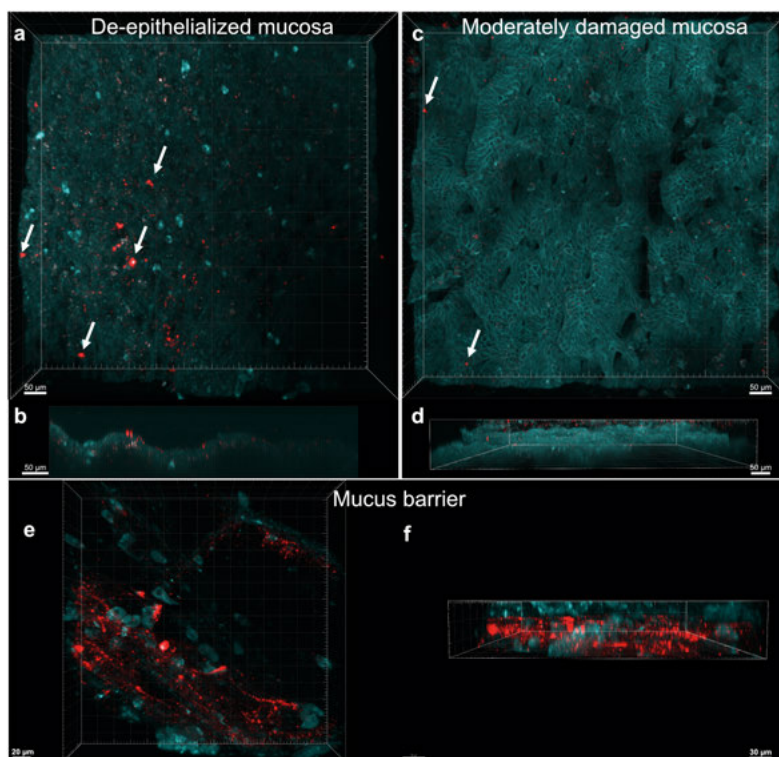


**Figure 23.** Fluorescence confocal images of colons from colitis-induced CFP transgenic mice depicted epithelial cells (cyan) and Ceacam1-conjugated particles (red). (a, c) Ceacam1-conjugated SPIONs (red) found in de-epithelialized area with severe crypt and epithelial loss in (c, d) Epithelial irregularities in moderately damaged mucosa. Arrows indicate SPION localization. (scale bar: (a-d) 50  $\mu\text{m}$ ). (e, f) Confocal microscopy of mucus layer with presence of agglomerates of Ceacam1-conjugated particles (red) demonstrated in overview (e) and cross-sectional (f) images (scale bar: (a) 20  $\mu\text{m}$  and (b) 30  $\mu\text{m}$ ).

Furthermore, the DBCO-conjugated linker enabled copper-free click chemistry for *in vivo* conjugation of SPIONs. These particles were hypothesized to exhibit enhanced dispersibility and permeation since they lack the antibody upon administration but are designed to conjugate with the targeting ligand *in vivo*. Confocal microscopy results appeared promising, indicating successful *in vivo* conjugation especially in de-epithelialized mucosa. However, a significant number of particles were trapped in the mucus layer, highlighting the complexity of overcoming biological barriers (Figure 24). This finding suggests that while the hydrodynamic diameter of these particles might have been smaller, they had a more negative surface charge that could hinder effective diffusion through the negatively charged mucus layer, as compared to the larger antibody-conjugated particles with near neutral surface charge.

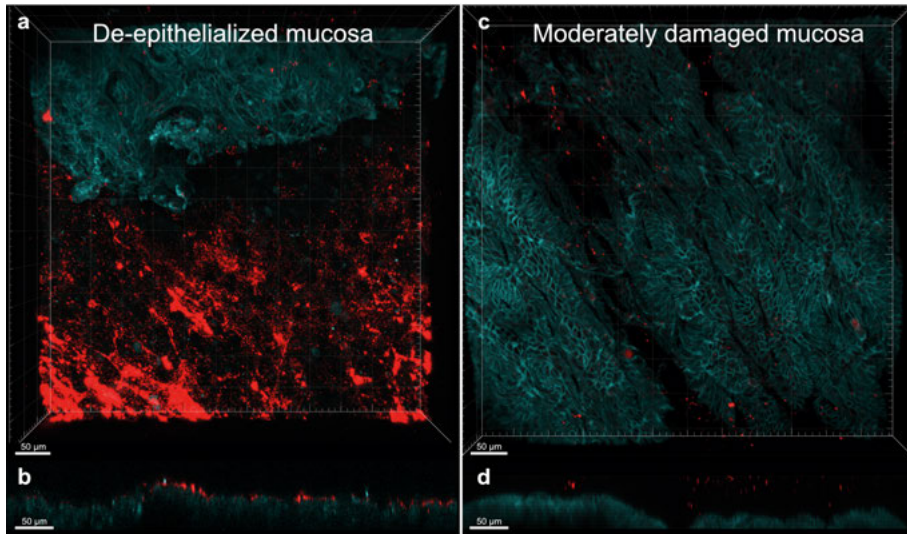


*Figure 24.* Fluorescence confocal images of colons from colitis-induced CFP reporter mice visualized epithelial cells (cyan) and DBCO-functionalized particles (red). (a, b) Severely damaged de-epithelialized mucosal tissue demonstrated large accumulation of particles along the underlying loose connective tissue. (c, d) In moderately damaged areas, SPION-COOH-DBCO were found in the mucus layer. (scale bars: 50µm)

### **Detection of bioconjugated nanoparticles *in vivo* using MRI**

Analysis of Ceacam1-targeted and DBCO-conjugated SPIONs in colitis-induced mice using MRI was conducted to evaluate their diagnostic potential to localize inflamed lesions in ulcerative colitis.

Fluorescent confocal microscopy provides a highly sensitive visualization of thin tissue slices, directly tracking the particles. In contrast, MRI detects signals from the relaxation of magnetic moments of water protons in the surrounding tissue, not the particles themselves. MRI generates 3D images, requiring volume considerations when comparing with microscopy images. Additionally, MRI is susceptible to artefacts such as air bubbles adhering to the tissue, which may produce signals not present in confocal microscopy.

Once volume differences were accounted for, overlapping signals were observed in both imaging techniques (Figure 25). Furthermore, a distinct difference in MRI signal (white) was noted between healthy (Figure 25b) and DSS-treated colitis-induced mice (Figure 25a). This highlights the enhanced contrast provided by Ceacam1-targeted SPIONs in inflamed tissue, supporting their potential utility for IBD diagnosis.

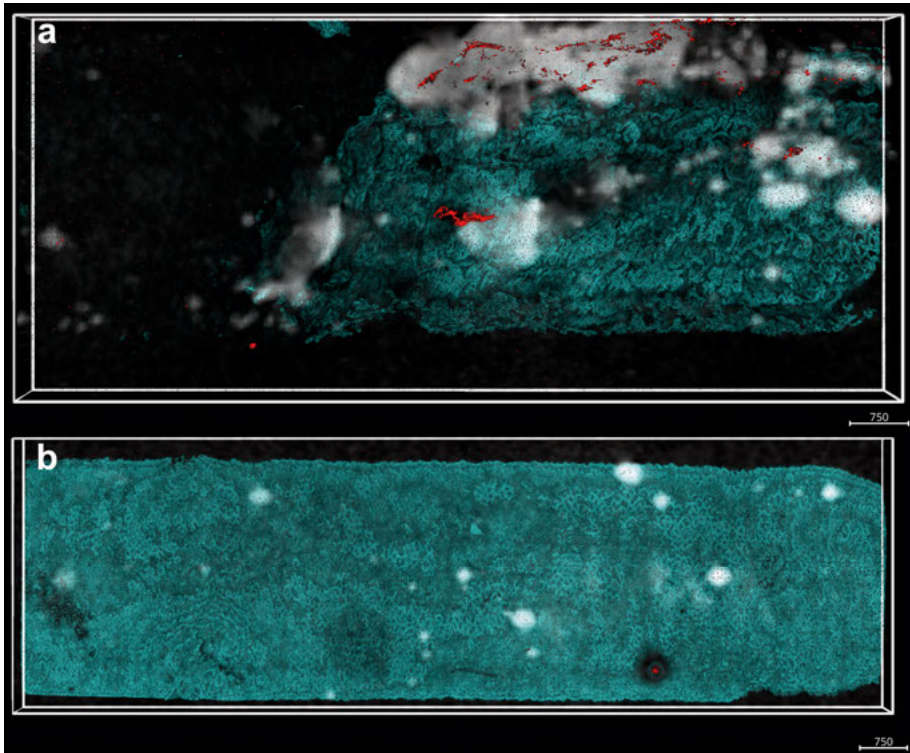


*Figure 25.* Overlaid images from MRI and confocal microscopy of colons from colitis-induced CFP reporter mice visualized epithelial cells (cyan) and SPION-COOH-alkyne-Ceacam1 (red). (a) DSS-treated and (b) healthy mice exposed to Ceacam1-conjugated particles. Rendered MRI contrast corresponds to white signal.

# Conclusions

This thesis includes the identification of preclinical IBD biomarkers, development and design of SPIONs targeting those biomarkers, and the utility of bioconjugated particles for targeted imaging and diagnostic applications in IBD. Through the introduction of functional groups and conjugation with specific antibodies, the potential for precise targeting and imaging in inflammatory conditions was assessed.

The specific conclusions of the thesis are:

- Global proteomics analysis identified upregulated inflammatory proteins Tgm2/TGM2, Ceacam1/CEACAM1, Icam1/ICAM1, and Anxa1/ANXA1 as common biomarkers in *in vitro* and *in vivo* IBD models, making them promising targets for diagnostic imaging probes (Paper I).
- Biomarkers such as Mpo, calprotectin (S100a8 and S100a9), Ltf, and Epx, were highly upregulated secreted proteins in the *in vivo* mouse model, providing quantitative information about IBD activity in the GI tract (Paper I).
- ICAM1-targeting antibodies were conjugated to alkyne-modified SPIONs using CuAAC. Characterization confirmed successful antibody conjugation, and TGA and SDS-PAGE analyses indicated that the use of a copper catalyst enhanced covalent bonding efficiency, reducing non-covalent antibody attachment (Paper II).
- ICAM-targeted SPIONs exhibited high biocompatibility in undifferentiated Caco-2 cells, with SiO<sub>2</sub> coating markedly enhancing cell viability (Paper II).
- Covalently conjugated SPIONs demonstrated significantly higher binding efficacy to inflamed Caco-2 cells compared to non-targeted or non-covalently conjugated particles, highlighting the importance of targeting ligands and covalent conjugation for specific binding (Paper II).
- Surface modifications of SPIONs with alkyne and carboxylic acid groups enabled smaller hydrodynamic diameter prior to bioconjugation using click chemistry, confirmed by DLS (Paper III).

- Antibodies targeting Icam1 and Ceacam1, biomarkers upregulated in IBD, were successfully conjugated to the SPIONs, as verified by hydrodynamic size, surface charge measurements and fluorescent labelling of alkynes (Paper III).
- An experimental protocol for rectal administration of bioconjugated SPIONs in mice was developed, demonstrating effective targeted delivery to the colon while bypassing the upper GI tract (Paper III).
- Imaging techniques revealed that Ceacam1-conjugated SPIONs preferentially accumulated in severely inflamed regions of the colon, providing insights into the severity and distribution of inflammation (Paper III).
- MRI of colons from mice exposed to Ceacam1-conjugated SPIONs demonstrated a distinct difference in signal between healthy and diseased mice, highlighting the enhanced contrast provided by targeted SPIONs in inflamed tissue. This supports their potential utility for IBD diagnosis (Paper III).

## Future perspectives

While the advancements in nanoparticle-based targeting are promising, several challenges remain. Ensuring the stability of targeted nanoparticles in the complex GI environment after oral administration is critical. One potential solution to protect the nanoparticle and its targeting moiety from the harsh GI conditions is by administering the nanoparticle system in enteric-coated capsules. This approach ensures that SPIONs are released in the small intestine, improving their stability and effectiveness in targeting inflamed tissues.

Additionally, understanding the long-term effects and potential toxicity of SPIONs is essential for their clinical translation. The ICAM1-conjugated SPIONs in this thesis demonstrated cellular interactions and internalization, making the concerns about long-term effects even more relevant. Future studies should focus on the identification of primary cellular uptake mechanisms, using e.g. chemical endocytosis inhibitors, building on previous findings that particles conjugated with ICAM1 predominantly utilize CAM-mediated pathways for internalization in Caco-2 cells. These observations highlight the internalization potential of functionalized SPIONs, necessitating further investigation into particle uptake mechanisms *in vitro*, as well as studying the metabolism and elimination of the particles *in vivo*.

In this thesis, overexpressed IBD targets were identified using global proteomics analysis, however, all of the found biomarkers were also present in healthy tissue. This highlights the challenges of identifying an optimal biomarker that enables differentiation between the healthy and inflamed state. Thus, a critical advancement would be the expansion of biomarkers, which could significantly enhance the accuracy of targeted diagnostics. Moreover, the integration of advanced bioinformatics and machine learning techniques can enhance the analysis and interpretation of proteomic data, leading to the discovery of novel biomarkers and therapeutic targets. Collaboration between multidisciplinary teams, including clinicians, biologists, and engineers, will be vital in driving these innovations from bench to bedside.

Furthermore, the development of nanoparticle-based strategies holds potential not only for early and accurate diagnosis of IBD but also for targeted drug delivery. This dual therapeutic and diagnostic ("theranostic") approach offers a comprehensive solution for managing GI diseases. By combining diagnostic imaging with targeted therapy, it is possible to monitor disease

progression and response to treatment more effectively, leading to improved patient outcomes.

In conclusion, the advancements in bioconjugated SPIONs for IBD diagnostics and treatment are paving the way for innovative, effective, and comprehensive approaches to managing GI diseases. The continuous research and development in this field promise to bring significant improvements in the accuracy of diagnosis and efficacy of treatments for IBD patients.

# Acknowledgements

The work in this thesis was carried out at the Department of Pharmacy, Uppsala University. The studies were financially supported by SciLifeLab and European Research Council (ERC). Anna Cederbergs stiftelse and Apotekare CD Carlssons stiftelse (Apotekasocieteten) are also gratefully acknowledged for travel grants that allowed me to take part in several research conferences.

*I would like to extend my heartfelt gratitude to the many individuals who have supported and assisted me throughout my studies. I owe special thanks to:*

My main supervisor, **Alexandra Teleki**. From the very beginning of my PhD journey, we often joked about how easily I was offered this position. At the time, I didn't fully grasp the significance of it, but as more members joined your group, it became clear that you took a leap of faith in offering me this opportunity without subjecting me to any rigorous knowledge tests or presentations. I am deeply grateful for your courage and for taking a risk on me as your first PhD student. Your trust and belief in my potential have been incredibly meaningful, and I am truly thankful for your support and guidance throughout this journey. You have witnessed all of my experimental setbacks and personal challenges over the past years, and I am deeply grateful for your help in lifting me back up after each one.

My co-supervisors, **Christel Bergström** and **Mia Phillipson**. You are both remarkable powerhouses who never seem to tire. Thank you for providing exceptional scientific support and invaluable knowledge throughout my studies. Your unwavering drive, scientific achievements and positive outlook on research have been truly inspiring to witness. Your feedback and kind words throughout the years have often provided the confidence boost I needed to persevere in my work. Thank you for your mentorship and encouragement.

My unofficial co-supervisor and friend, **Máté Erdélyi**. Thank you for planting the seed and encouraging me to pursue a PhD. I am deeply grateful for the lunches and tea breaks that you somehow managed to fit into your busy schedule. Your humble outlook on life has kept me grounded throughout the years. Your advice has guided me through both professional challenges and personal

dilemmas and I am thankful for the invaluable insights you have shared with me.

My co-author and friend, **David Ahl**. Through our collaborations, I have gained more knowledge than I ever imagined during my studies. Everything I know about animal studies, I owe to you. While you may not see yourself as a role model, you have become someone I admire and look up to. During times when everything seemed to fail, you have been the rock to lean on. Thank you for the countless moments of laughter and joy that you have brought me over the past years; our work together has been the highlight of my time here.

My colleague and cell work advisor, **Maria Karlgren**. Thank you for dedicating your time to instructing me in cell work. Your expertise and guidance have proven invaluable to the progress of my research. I deeply appreciate the insights and knowledge you have shared, which have significantly enriched my work and understanding in this field.

My former professor and supervisor, **Morten Grøtli**. Thank you for introducing me to the world of research by welcoming me as an undergraduate student in your group. Your mentorship and guidance were contributory in securing this PhD position. The knowledge and skills I have acquired during my PhD studies are a direct result of your support and encouragement. I am grateful for the foundation you provided, which has been crucial for my academic and professional development.

To all the former and present members of the BLT-group, thank you for meaningful discussions and support throughout my PhD studies.

**Shaquib**: My first nano-colleague, thank you for joining the team and becoming a good friend. I truly value our insightful discussions about life and research. Fond memories of our spontaneous breaks to enjoy churros or ice cream will always bring a smile to my face.

**Yuming**: You have a remarkable ability to brighten every room you enter, and I feel incredibly fortunate to have crossed paths with you on this journey. Thank you for embracing my sense of humour and for infusing the lab with your contagious energy and joy each day. I can't imagine my time here without you; your friendship has been a cornerstone of my PhD experience.

**Jiayi**: Your thoughtfulness and kindness during my struggles has consistently lifted my spirits. I deeply appreciate your invaluable friendship and for always being there to listen to my complaints and concerns.

**Mingjun**: Thank you for being such a sweet and funny colleague and friend. Despite your quiet demeanour, your sense of humour never fails to make me laugh, and your presence is always missed when you're not around.

**Marco**: I truly appreciate your patience and not reporting me to HR or the equal opportunities group during all these years.

**Lidia:** Your infectious laughter has brightened even the toughest days. Thank you for being such a caring and helpful colleague and friend.

**Merve:** Thank you for sharing all of your crazy stories and for always bringing so much laughter during the past years.

**Yael:** Your positive personality has made our work both productive and enjoyable. I appreciate your easy-going nature and for your persistent motivation to one day get me to join you for climbing.

**Lingxiao:** Your constantly positive attitude is a joy to be around, thank you for your uplifting words whenever those have been necessary.

**Malhar:** Finding snacks and chocolates on my desk when entering the office was always a delightful surprise, brightening even the darkest days. Thank you for fuelling my late-night sessions with such thoughtful gestures.

**Xiguo:** Thank you for being an amazing office mate and for all of the chocolate and lovely gifts. I have truly enjoyed our discussions and conversations over the years. Your presence has made the office a much brighter place.

**Aleksei:** Thank you for always being such a great source of positivity and for always engaging in discussions that interest me, even when I know you don't always find them amusing.

**Shakhawath:** A tremendous thank you for putting up with my frequent "emergency orders". None of the work in this thesis would have been accomplished without your help.

**Paarkavi:** Thank you for inviting me to all the get-togethers and events that has happened during the past years. Although I often couldn't attend, I truly appreciated the gesture.

Thank you to **Shahina, Mira** and **Benyamin** for being such hardworking and fun colleagues, you guys are truly admirable. Finally, thank you to **Caroline, Albin, Oliver** and **Vicky** for being the great seniors I could look up to when I started my PhD. I have enjoyed our discussions, which have been helpful in many ways, both professionally and personally.

Till mina vänner som har varit med varje steg på vägen.

**Yasamin:** Jag må ha blandade känslor gällandes min tid i Uppsala, men jag skulle aldrig ändra något, då det skulle potentiellt innebära att jag inte hade fått möjligheten att utveckla kontakten jag har med dig idag. Vår tid tillsammans på BMC var kortvarig, men resulterade i en fantastisk vänskap som inte går att värdesätta. Tack för ditt stöd och dina konstant upplyftande ord. Du har betytt mer än du kan ana.

**Krenare:** Trots ditt hektiska schema och den långa distansen har du lyckats besöka mig i Uppsala flera gånger, vilket jag är oerhört tacksam för. Dina besök och våra långa telefonsamtal har alltid gett mig ny energi och motivation att fortsätta. Tack för ditt ovärderliga stöd.

**Twana:** Stort tack för att du alltid har tagit dig tid att lyssna på mina experimentella problem och engagerat dig i att förstå min forskning. Din vilja att

fungera som ett bollplank och bidra med dina insikter har varit ovärderlig. Jag uppskattar ditt stöd och dina kloka råd mer än jag kan uttrycka i ord.

**Sara:** Du följde med mig till Uppsala inför min första intervju för denna doktorandtjänst, och din närvaro har fortsatt vara en konstant källa till stöd genom varje steg på denna resa. Du har besökt mig mer än någon annan, och tack vare dig har jag aldrig känt mig ensam. Din närvaro och ditt engagemang har varit ovärderliga, och jag har alltid kunnat vända mig till dig när jag behövt stöd eller råd. Tack för att du har varit min tryggaste punkt genom alla dessa år, och för att du alltid funnits där för mig.

Till min underbara familj, utan er vore jag ingenting.

Tack till mina fantastiska föräldrar, som har varit min främsta källa till motivation under alla dessa år. Inte en enda dag har gått utan att ni har ringt mig för att visa er omtanke och stöd. Min frys har aldrig stått tom tack vare er, och er villkorslösa kärlek har gett mig kraften och motivation till att alltid göra mitt bästa. Ert stöd har varit ovärderligt och jag är oändligt tacksam för allt ni har gjort för mig. Ett stort tack till **Sham, Karwan** och **Sokar** för ert stöd och närvaro. Er uppmuntran har betytt oerhört mycket för mig under denna resa och jag är tacksam som haft er vid min sida.

# References

- [1] K. Riehemann, S. W. Schneider, T. A. Luger, B. Godin, M. Ferrari, H. Fuchs, *Angew Chem* **2009**, *48*, 872.
- [2] C. Zhang, L. Yan, X. Wang, S. Zhu, C. Chen, Z. Gu, Y. Zhao, *Nano Today* **2020**, *35*, 101008.
- [3] P. N. Navya, H. K. Daima, *Nano Converge* **2016**, *3*, 1.
- [4] M. J. Mitchell, M. M. Billingsley, R. M. Haley, M. E. Wechsler, N. A. Peppas, R. Langer, *Nat Rev Drug Discov* **2021**, *20*, 101.
- [5] D. C. Baumgart, S. R. Carding, *Lancet* **2007**, *69*, 1627
- [6] S. Alatab, S. G. Sepanlou, K. Ikuta, H. Vahedi, C. Bisignano, S. Safiri, A. Sadeghi, M. R. Nixon, A. Abdoli, H. Abolhassani, V. Alipour, M. A. H. Almadi, A. Almasi-Hashiani, A. Anushiravani, J. Arabloo, S. Atique, A. Awasthi, A. Badawi, A. A. A. Baig, N. Bhala, A. Bijani, A. Biondi, A. M. Borzi, K. E. Burke, F. Carvalho, A. Daryani, M. Dubey, A. Eftekhari, E. Fernandes, J. C. Fernandes, F. Fischer, A. Haj-Mirzaian, A. Haj-Mirzaian, A. Hasanzadeh, M. Hashemian, S. I. Hay, C. L. Hoang, M. Househ, O. S. Ilesanmi, N. J. Balalami, S. L. James, A. P. Kengne, M. M. Malekzadeh, S. Merat, T. J. Meretoja, T. Mestrovic, E. M. Mirrakhimov, H. Mirzaei, K. A. Mohammad, A. H. Mokdad, L. Monasta, I. Negoii, T. H. Nguyen, C. T. Nguyen, A. Pourshams, H. Poustchi, M. Rabiee, N. Rabiee, K. Ramezanzadeh, D. L. Rawaf, S. Rawaf, N. Rezaei, S. R. Robinson, L. Ronfani, S. Saxena, M. Sepehrimanesh, M. A. Shaikh, Z. Sharafi, M. Sharif, S. Siabani, A. R. Sima, J. A. Singh, A. Soheili, R. Sotoudehmanesh, H. A. R. Suleria, B. E. Tesfay, B. Tran, D. Tsoi, M. Vacante, A. B. Wondmieneh, A. Zarghi, Z. J. Zhang, M. Dirac, R. Malekzadeh, M. Naghavi, *Lancet Gastroenterol Hepatol* **2020**, *5*, 17.
- [7] R. Wang, Z. Li, S. Liu, D. Zhang, *BMJ Open* **2023**, *13*, e065186.
- [8] S. C. Ng, H. Y. Shi, N. Hamidi, F. E. Underwood, W. Tang, E. I. Benchimol, R. Panaccione, S. Ghosh, J. C. Y. Wu, F. K. L. Chan, J. J. Y. Sung, G. G. Kaplan, *The Lancet* **2017**, *390*, 2769.
- [9] G. G. Kaplan, J. W. Windsor, *Nat Rev Gastroenterol Hepatol* **2021**, *18*, 56.
- [10] Z. Cai, S. Wang, J. Li, *Front Med (Lausanne)* **2021**, *8*, 765474.
- [11] K. O. Chudy-Onwugaje, K. E. Christian, F. A. Farraye, R. K. Cross, *Inflamm Bowel Dis* **2019**, *25*, 820.
- [12] R. W. Katia, E. J. Nada, Z. David, T. Rubin, *Adv Ther* **2018**, *35*, 1746.
- [13] G. Fiorino, S. Danese, *Dig Dis Sci* **2016**, *61*, 3097.
- [14] N. Jayasooriya, S. Baillie, J. Blackwell, A. Bottle, I. Petersen, H. Creese, S. Saxena, R. C. Pollok, *Aliment Pharmacol Ther* **2023**, *57*, 635.
- [15] L. Y. Mak, T. S. M. Tong, K. S. Cheung, L. J. Chen, K. L. Lui, K. S. Lau, W. K. Leung, *Clin Transl Gastroenterol* **2020**, *11*, e00138.

- [16] C. G. B. Peterson, M. Lampinen, T. Hansson, M. Lidén, R. Hällgren, M. Carlson, *Scand J Clin Lab Invest* **2016**, *76*, 393.
- [17] M. Dai, T. Zhang, Q. Li, B. Cui, L. Xiang, X. Ding, R. Rong, J. Bai, J. Zhu, F. Zhang, *Trials* **2019**, *20*, 1.
- [18] A. Laghi, P. Paolantonio, F. Altomari, C. Miglio, R. Passariello, *Top Magn Reson Imaging*, **2002**, *13*, 389
- [19] E. M. Materón, C. M. Miyazaki, O. Carr, N. Joshi, P. H. S. Picciani, C. J. Dalmaschio, F. Davis, F. M. Shimizu, *Appl Surf Sci Adv* **2021**, *6*, 100163.
- [20] A. Farzin, S. A. Etesami, J. Quint, A. Memic, A. Tamayol, *Adv Healthc Mater* **2020**, *9*, 1901058.
- [21] M. Mahmoudi, S. Sant, B. Wang, S. Laurent, T. Sen, *Adv Drug Deliv Rev* **2011**, *63*, 24.
- [22] J. Dulińska-Litewka, A. Łazarczyk, P. Hałubiec, O. Szafranski, K. Karnas, A. Karewicz, *Materials* **2019**, *12*, 617.
- [23] C. Xu, S. Sun, *Adv Drug Deliv Rev* **2013**, *65*, 732.
- [24] M. Nabavinia, J. Beltran-Huarac, *ACS Appl Bio Mater* **2020**, *3*, 8172.
- [25] Y. Li, D. Ye, M. Li, M. Ma, N. Gu, *ChemPhysChem* **2018**, *19*, 1965.
- [26] P. Kaur, M. L. Aliru, A. S. Chadha, A. Asea, S. Krishnan, *Int J Hyperth* **2016**, *32*, 76.
- [27] R. Jin, B. Lin, D. Li, H. Ai, *Curr Opin Pharmacol* **2014**, *18*, 18.
- [28] Y. Bao, J. A. Sherwood, Z. Sun, *J Mater Chem C Mater* **2018**, *6*, 1280.
- [29] Z. R. Stephen, F. M. Kievit, M. Zhang, *Mater Today* **2011**, *14*, 330.
- [30] R. Qiao, C. Yang, M. Gao, *J Mater Chem* **2009**, *19*, 6274.
- [31] M. Dai, T. Zhang, Q. Li, B. Cui, L. Xiang, X. Ding, R. Rong, J. Bai, J. Zhu, F. Zhang, *Trials* **2019**, *20*, 1.
- [32] B. K. Sodipo, A. A. Aziz, *J Magn Magn Mater* **2016**, *416*, 275.
- [33] C. R. Lin, Y. M. Chu, S. C. Wang, *Mater Lett* **2006**, *60*, 447.
- [34] A. Ali, H. Zafar, M. Zia, I. ul Haq, A. R. Phull, J. S. Ali, A. Hussain, *Nanotechnol Sci Appl* **2016**, *9*, 49.
- [35] A. Teleki, M. Suter, P. R. Kidambi, O. Ergeneman, F. Krumeich, B. J. Nelson, S. E. Pratsinis, *Chem Mater* **2009**, *21*, 2094.
- [36] A. Teleki, F. L. Haufe, A. M. Hirt, S. E. Pratsinis, G. A. Sotiriou, *RSC Adv* **2016**, *6*, 21503.
- [37] S. R. Ansari, Y. del C. Suárez-López, T. Thersleff, L. Häggström, T. Ericsson, I. Katsaros, M. Åhlén, M. Karlgren, P. Svedlindh, C. M. Rinaldi-Ramos, A. Teleki, *ACS Nano* **2024**, *18*, 15284.
- [38] M. Arruebo, M. Valladares, Á. González-Fernández, *J Nanomater* **2009**, *2009*, 439389.
- [39] X. Lin, A. O'Reilly Beringhs, X. Lu, *AAPS Journal* **2021**, *23*, 43.
- [40] Y. Gao, S. Gu, Y. Zhang, X. Xie, T. Yu, Y. Lu, Y. Zhu, W. Chen, H. Zhang, H. Dong, P. J. Sinko, L. Jia, *Small* **2016**, *12*, 2595.
- [41] R. T. Busch, F. Karim, J. Weis, Y. Sun, C. Zhao, E. S. Vasquez, *ACS Omega* **2019**, *4*, 15269.
- [42] K. Werengowska-Ciećwierz, M. Wiśniewski, A. P. Terzyk, S. Furmaniak, *J. Condens Matter Phys* **2015**, *2015*, *10*, 198175.
- [43] T. J. Yoon, K. N. Yu, E. Kim, J. S. Kim, B. G. Kim, S. H. Yun, B. H. Sohn, M. H. Cho, J. K. Lee, S. B. Park, *Small* **2006**, *2*, 209.
- [44] N. K. Lee, C. P. J. Wang, J. Lim, W. Park, H. K. Kwon, S. N. Kim, T. H. Kim, C. G. Park, *Nano Converg* **2021**, *8*, 24.
- [45] C. Ndong, S. Toraya-Brown, K. Kekalo, I. Baker, T. U. Gerngross, S. N. Fiering, K. E. Griswold, *Int J Nanomedicine* **2015**, *10*, 2595.

- [46] C. Finetti, L. Sola, M. Pezzullo, D. Prosperi, M. Colombo, B. Riva, S. Avvakumova, C. Morasso, S. Picciolini, M. Chiari, *Langmuir* **2016**, *32*, 7435.
- [47] D. L. J. Thorek, D. R. Elias, A. Tsourkas, *Mol Imaging* **2009**, *8*, 221.
- [48] S. Jeong, J. Y. Park, M. G. Cha, H. Chang, Y. il Kim, H. M. Kim, B. H. Jun, D. S. Lee, Y. S. Lee, J. M. Jeong, Y. S. Lee, D. H. Jeong, *Nanoscale* **2017**, *9*, 2548.
- [49] T. Kim, H. N. Hyun, R. Heo, K. Nam, K. Yang, Y. M. Kim, Y. S. Lee, J. Y. An, J. H. Park, K. Y. Choi, Y. H. Roh, *ChemComm* **2020**, *56*, 6624.
- [50] M. Rashidian, J. K. Dozier, M. D. Distefano, *Bioconjug Chem* **2013**, *24*, 1277.
- [51] P. Artursson, *J Pharm Sci* **1990**, *79*, 476.
- [52] I. Hubatsch, E. G. E. Ragnarsson, P. Artursson, *Nat Protoc* **2007**, *2*, 2111.
- [53] Y. Araki, H. Sugihara, T. Hattori, *Oncol Rep* **2006**, *16*, 1357.
- [54] J. Van De Walle, A. Hendrickx, B. Romier, Y. Larondelle, Y. J. Schneider, *In vitro Toxicol* **2010**, *24*, 1441.
- [55] B. Chassaing, J. D. Aitken, M. Malleshappa, M. Vijay-Kumar, *Curr Protoc Immunol* **2014**, *104*, 1525s1.
- [56] H. S. Cooper, S. N. Murthy, R. S. Shah, D. J. Sedergran, *Lab Invest* **1993**, *69*, 238.
- [57] J. R. Wiśniewski, M. Mann, *Anal Chem* **2012**, *84*, 2631.
- [58] J. R. Wiśniewski, F. Z. Gaugaz, *Anal Chem* **2015**, *87*, 4110.
- [59] S. Tyanova, T. Temu, J. Cox, *Nat Protoc* **2016**, *11*, 2301.
- [60] J. R. Wiśniewski, D. Rakus, *Data Brief* **2014**, *1*, 7.
- [61] M. E. Ritchie, B. Phipson, D. Wu, Y. Hu, C. W. Law, W. Shi, G. K. Smyth, *Nucleic Acids Res* **2015**, *43*, e47.
- [62] G. Yu, L. G. Wang, Y. Han, Q. Y. He, *OMICS* **2012**, *16*, 284.
- [63] B. Chassaing, J. D. Aitken, M. Malleshappa, M. Vijay-Kumar, *Curr Protoc Immunol* **2014**, *104*, 1525s1
- [64] K.-W. Chang, C.-Y. Kuo, *Food Funct*, **2015**, *6*, 3334.
- [65] Y. Araki, H. Sugihara, T. Hattori, *Oncol Rep* **2006**, *16*, 1357.
- [66] M. H. Sheikh, E. Solito, *Int J Mol Sci* **2018**, *19*, 1904.
- [67] Z. Zou, D. Zuo, J. Yang, H. Fan, *Biochem Biophys Res Commun* **2016**, *478*, 213.
- [68] G. Roda, S. Dahan, L. Mezzanotte, A. Caponi, F. Roth-Walter, D. Pinn, L. Mayer, *Inflamm Bowel Dis* **2009**, *15*, 1775.
- [69] W. Reinisch, K. Hung, M. Hassan-Zahraee, F. Cataldi, *J Crohns Colitis* **2018**, *12*, S669.
- [70] R. Sumagin, J. C. Brazil, P. Nava, H. Nishio, A. Alam, A. C. Luissint, D. A. Weber, A. S. Neish, A. Nusrat, C. A. Parkos, *Mucosal Immunol* **2016**, *9*, 1151.
- [71] L. Elli, M. M. Ciulla, G. Busca, L. Roncoroni, C. Maioli, S. Ferrero, M. T. Bardella, A. Bonura, R. Paliotti, C. Terrani, P. Braidotti, *Lab Invest* **2011**, *91*, 452.
- [72] B. Chami, N. J. J. Martin, J. M. Dennis, P. K. Witting, *Arch Biochem Biophys* **2018**, *645*, 61.
- [73] B. Chen, A. L. Miller, M. Rebelatto, Y. Brewah, D. C. Rowe, L. Clarke, M. Czapiga, K. Rosenthal, T. Imamichi, Y. Chen, C. S. Chang, P. S. Chowdhury, B. Naiman, Y. Wang, D. Yang, A. A. Humbles, R. Herbst, G. P. Sims, *PLoS One* **2015**, *10*, e0115828.

- [74] M. Pruenster, T. Vogl, J. Roth, M. Sperandio, *Pharmacol Ther* **2016**, *167*, 120.
- [75] J. Dai, W. Z. Liu, Y. P. Zhao, Y. B. Hu, Z. Z. Ge, *Scand J Gastroenterol* **2007**, *42*, 1440.
- [76] O. Saitoh, K. Kojima, K. Sugi, R. Matsuse, K. Uchida, K. Tabata, K. Nakagawa, M. Kayazawa, I. Hirata, K. Katsu, *Am J Gastroenterol* **1999**, *94*, 3513.
- [77] J. Estelrich, M. J. Sánchez-Martín, M. A. Busquets, *Int J Nanomedicine* **2015**, *10*, 1727.
- [78] H. P. Le Khanh, D. Nemes, Á. Ruzsnyák, Z. Ujhelyi, P. Fehér, F. Fenyvesi, J. Váradi, M. Vecsernyés, I. Bácskay, *Polymers (Basel)* **2022**, *14*, 279.
- [79] G. Liu, Y. Li, L. Yang, Y. Wei, X. Wang, Z. Wang, L. Tao, *RSC Adv* **2017**, *7*, 18252.
- [80] S. J. Soenen, B. B. Manshian, A. M. Abdelmonem, J. M. Montenegro, S. Tan, L. Balcaen, F. Vanhaecke, A. R. Brisson, W. J. Parak, S. C. De Smedt, K. Braeckmans, *Part Syst Charact* **2014**, *31*, 794.
- [81] S. A. A. Rizvi, A. M. Saleh, *SPJ* **2018**, *26*, 64.
- [82] G. M. H. Birchenough, E. E. L. Nyström, M. E. V Johansson, G. C. Hansson, *Science* **2016**, *352*, 1535.
- [83] S. Van Der Post, K. S. Jabbar, G. Birchenough, L. Arike, N. Akhtar, H. Sjøvall, M. E. V. Johansson, G. C. Hansson, *Gut* **2019**, *68*, 2142.



# Acta Universitatis Upsaliensis

*Digital Comprehensive Summaries of Uppsala Dissertations from the Faculty of Pharmacy 355*

Editor: The Dean of the Faculty of Pharmacy

A doctoral dissertation from the Faculty of Pharmacy, Uppsala University, is usually a summary of a number of papers. A few copies of the complete dissertation are kept at major Swedish research libraries, while the summary alone is distributed internationally through the series Digital Comprehensive Summaries of Uppsala Dissertations from the Faculty of Pharmacy. (Prior to January, 2005, the series was published under the title “Comprehensive Summaries of Uppsala Dissertations from the Faculty of Pharmacy”.)

Distribution: [publications.uu.se](http://publications.uu.se)  
urn:nbn:se:uu:diva-532431



ACTA UNIVERSITATIS  
UPSALIENSIS  
2024